



HAL
open science

Role of the *Escherichia coli* ubiquinone-synthesizing UbiUVT pathway in adaptation to changing respiratory conditions

Arias-Cartin Rodrigo, Kazemzadeh Ferizhendi Katayoun, Séchet Emmanuel, Pelosi Ludovic, Loeuillet Corinne, Pierrel Fabien, Barras Frédéric, Bouveret Emmanuelle

► **To cite this version:**

Arias-Cartin Rodrigo, Kazemzadeh Ferizhendi Katayoun, Séchet Emmanuel, Pelosi Ludovic, Loeuillet Corinne, et al. Role of the *Escherichia coli* ubiquinone-synthesizing UbiUVT pathway in adaptation to changing respiratory conditions. 2023. pasteur-04109372

HAL Id: pasteur-04109372

<https://pasteur.hal.science/pasteur-04109372>

Preprint submitted on 30 May 2023

HAL is a multi-disciplinary open access archive for the deposit and dissemination of scientific research documents, whether they are published or not. The documents may come from teaching and research institutions in France or abroad, or from public or private research centers.

L'archive ouverte pluridisciplinaire **HAL**, est destinée au dépôt et à la diffusion de documents scientifiques de niveau recherche, publiés ou non, émanant des établissements d'enseignement et de recherche français ou étrangers, des laboratoires publics ou privés.

Copyright

1 **Role of the *Escherichia coli* ubiquinone-synthesizing UbiUVT pathway in**
2 **adaptation to changing respiratory conditions**

3

4 Arias-Cartin Rodrigo^{1*}, Kazemzadeh Ferizhendi Katayoun^{2*}, Séchet Emmanuel^{1*}, Pelosi
5 Ludovic², Loeuillet Corinne³, Pierrel Fabien², Barras Frédéric^{1#} and Bouveret Emmanuelle^{1#}

6

7 ¹ Institut Pasteur, Département de Microbiologie, Université Paris-Cité, UMR CNRS 6047,
8 SAME Unit, Institut Pasteur, France.

9 ² Univ. Grenoble Alpes, CNRS, UMR 5525, VetAgro Sup, Grenoble INP, TIMC, 38000
10 Grenoble, France.

11 ³ Univ. Grenoble Alpes, INSERM U1209, CNRS UMR 5309, Institute for Advanced Biosciences,
12 Team Genetics Epigenetics and Therapies of Infertility, 38000 Grenoble, France.

13

14

15 * All three authors contributed equally to this work and their names appear in alphabetical
16 order

17

18 # co-corresponding authors: fbarras@pasteur.fr ; emmanuelle.bouveret@pasteur.fr

19

20 This study is dedicated to the memory of our friend and colleague Professor Josep
21 Casadesús.

22

23

24

25 **Keywords :** quinone – *E. coli* – Fnr – respiration - UbiTUV

26 **ABSTRACT**

27

28 Isoprenoid quinones are essential for cellular physiology. They act as electron and proton
29 shuttles in respiratory chains and in various biological processes. *Escherichia coli* and many
30 α , β , and γ proteobacteria possess two types of isoprenoid quinones: ubiquinone (UQ) is
31 mainly used under aerobiosis, while (demethyl)menaquinones ((D)MK) are mostly used
32 under anaerobiosis. Yet, we recently established the existence of an anaerobic O₂-
33 independent UQ biosynthesis pathway controlled by *ubiT*, *ubiU*, and *ubiV* genes. Here, we
34 characterize the regulation of *ubiTUV* genes in *E. coli*. We show that the three genes are
35 transcribed as two divergent operons that are both under the control of the O₂ sensing Fnr
36 transcriptional regulator. Phenotypic analyses using a *menA* mutant devoid of (D)MK
37 revealed that UbiUV-dependent UQ synthesis is essential for nitrate respiration and for
38 uracil biosynthesis under anaerobiosis, while it contributes, though modestly, to bacterial
39 multiplication in the mouse gut. Moreover, we showed by genetic study and ¹⁸O₂ labelling
40 that UbiUV contribute to hydroxylation of ubiquinone precursors through a unique O₂ -
41 independent process. Last, we report a crucial role of *ubiT* in allowing *E. coli* to shift
42 efficiently from anaerobic to aerobic conditions. Overall, this study uncovers a new facet of
43 the strategy used by *E. coli* to adjust its metabolism upon changing O₂ levels and respiratory
44 conditions. This work links respiratory mechanisms to phenotypic adaptation, a major driver
45 in the capacity of *E. coli* to multiply in gut microbiota, and of facultative anaerobic pathogens
46 to multiply in their host.

47

48 **ABSTRACT IMPORTANCE**

49 Enterobacteria multiplication in the gastrointestinal tract is linked to microaerobic
50 respiration and associated to various inflammatory bowel diseases. Our study focuses on
51 biosynthesis of ubiquinone (UQ), a key player in respiratory chains, under anaerobiosis. The
52 importance of this study stems from the fact that UQ usage was for long considered to be
53 restricted to aerobic conditions. Here we investigated the molecular mechanism allowing UQ
54 synthesis in the absence of O₂ and searched for the anaerobic processes that UQ is fueling in
55 such conditions. We found that UQ biosynthesis involves anaerobic hydroxylases, i.e.
56 enzymes able to insert a O atom in the absence of O₂. We also found that anaerobically
57 synthesized UQ can be used for respiration on nitrate and synthesis of pyrimidine. Our
58 findings are likely to be applicable to most facultative anaerobes, which count many
59 pathogens (Salmonella, Shigella, Vibrio) and will help in unravelling microbiota dynamics.

60

61 INTRODUCTION

62 Isoprenoid quinones are widely distributed in the three domains of life and globally act as
63 electron and proton carriers (1). They serve in many processes of bacterial physiology and
64 electron transport chains like photosynthesis, e.g. plastoquinone and phylloquinone, and
65 respiration, e.g. ubiquinone (UQ) and menaquinone (MK) (2). Isoprenoid quinones are
66 composed of a quinone ring and a poly-isoprenoid side chain whose length varies between
67 organisms (for instance UQ₈ in *Escherichia coli* and UQ₉ in *Pseudomonas aeruginosa*). Many
68 proteobacteria, such as *E. coli*, produce two main types of quinones: benzoquinones,
69 represented by UQ, and naphthoquinones, such as MK and demethyl-menaquinone (DMK).
70 In respiratory chains, quinones transfer electrons from primary dehydrogenases to terminal
71 reductases. For decades, *E. coli* aerobic and anaerobic respiratory chains were thought to
72 rely on UQ and MK/DMK, respectively. Yet, we have recently discovered a new pathway for
73 UQ biosynthesis under anaerobiosis, opening the way to a more complex and redundant
74 model for bacterial respiratory metabolism (3).

75 Aerobic UQ biosynthesis pathway includes 9 steps (4) (Figure S1). It begins with the
76 conversion of chorismate to 4-hydroxybenzoate (4HB) by the chorismate lyase UbiC. Then,
77 the phenyl ring of the 4HB precursor undergoes condensation with a 40-carbon long
78 isoprenoid chain in a reaction catalyzed by the UbiA enzyme. Subsequently, a series of
79 modifications on the 4HB ring by two methylases (UbiE and UbiG), a two-component
80 decarboxylase (UbiD, UbiX), and three hydroxylases (UbiI, UbiH and UbiF) generate the final
81 UQ₈ product. The FAD-monooxygenases UbiI, UbiH, and UbiF use molecular O₂ for their
82 hydroxylation reaction (5–7). An atypical kinase-like protein called UbiB is also involved in
83 UQ₈ synthesis, but its exact role remains elusive (8). In addition, two non-enzymatic factors
84 are required, UbiJ and UbiK, which may allow UbiI-EFGH enzymes to assemble in a
85 cytoplasmic 1 MDa complex, referred to as the Ubi metabolon (9). Also, UbiJ and UbiK bind
86 lipids, which may help the hydrophobic UQ biosynthesis to proceed inside a hydrophilic
87 environment.

88 Anaerobic UQ biosynthesis is formed by a subset of the enzymes of the aerobic
89 pathway, namely UbiA, UbiB, UbiC, UbiD, UbiE, UbiG and UbiX, that function with UbiT,
90 UbiU, and UbiV proteins solely required under anaerobiosis (3) (Figure S1). Like its homolog
91 counterpart UbiJ, UbiT contains a SCP2 lipid-binding domain. Strikingly, UbiU and UbiV do

92 not exhibit any sequence similarity or functional relatedness with the hydroxylases UbiI,
93 UbiH, or UbiF. UbiU and UbiV each contain an iron-sulfur ([4Fe-4S]) cluster coordinated by
94 four conserved cysteine residues embedded in the so-called protease U32 domain, and they
95 form a soluble UbiUV complex (3). Interestingly, two other members of the U32 protein
96 family, RlhA and TrhP, are involved in hydroxylation reactions. They introduce specific
97 nucleotide modifications respectively in the 23S rRNA or in some tRNAs (10–12).

98 In this work, we aimed at identifying the conditions under which UbiUVT proteins are
99 produced and the genetic regulatory mechanisms involved, and the physiological role of
100 UbiTUV. We concluded that (i) thanks to Fnr control, UbiUV ensure the production of UQ
101 under a range of O₂ levels, from anaerobiosis to microaerobiosis, (ii) a dual
102 anaerobic/aerobic regulation allows UbiT to secure a rapid shift from anaerobic UbiUV-
103 dependent UQ synthesis to an aerobic UbiIHF-dependent UQ synthesis, and (iii) UbiUV-
104 synthesized UQ can be used for nitrate respiration and anaerobic pyrimidine biosynthesis.
105 We also showed that UbiUV act as O₂-independent hydroxylases paving the way for future
106 studies towards the characterization of a new type of chemistry.

107

108 RESULTS

109

110 1. Biochemical function of UbiUV *in vivo*

111 To get further insight into the UbiUVT system *in vivo*, we tested whether overproduction of
112 UbiU and UbiV could substitute for the three oxygen-dependent hydroxylases UbiI, UbiH, or
113 UbiF. Thus, we cloned the *ubiUV* operon in the pBAD24 vector downstream the arabinose
114 inducible pBAD promoter (pES154 plasmid). In parallel, we also cloned *ubiUV* upstream the
115 SPA tag encoding sequence in order to assess the quantities of proteins produced. The
116 pBAD-*ubiUV*-SPA plasmid produces a level of UbiV protein approximately 30-fold higher to
117 that produced by a chromosomal copy of *ubiV-SPA* under anaerobiosis (Figure S2). After
118 transformation of mutant strains, selection, and precultures with LB medium in absence of
119 O₂, growth on M9 succinate was tested as it strictly depends upon an aerobic UQ-dependent
120 respiratory chain (Figure 1). In the presence of inducer, the pES154 plasmid was able to
121 suppress the growth phenotype of the $\Delta ubiF$, $\Delta ubiH$, $\Delta ubiIK$, and $\Delta ubiIHF$ mutants (Figure
122 1A). Note that as a control, we used the *Neisseria meningitidis ubiM* gene that we previously
123 showed to substitute for the growth phenotype of a $\Delta ubiIHF$ mutant (13). Also, in M9
124 succinate, the $\Delta ubiI$ mutation alone has no growth phenotype and needs to be combined
125 with $\Delta ubiK$ mutation for a defect to be observed (14). To test the importance of the UbiU-
126 bound [Fe-S] cluster, a complementation test was carried out in the same conditions, using a
127 pBAD derivative carrying the *ubiU*(C176A) allele that produces an UbiU variant lacking its
128 [Fe-S] cluster (3). Accordingly, suppression of $\Delta ubiH$, $\Delta ubiF$, $\Delta ubiIK$, and $\Delta ubiIHF$ was no
129 longer observed (Figure 1A). In addition, the pES154 plasmid was unable to suppress the
130 growth phenotype of $\Delta ubiA$, $\Delta ubiD$, $\Delta ubiE$, or $\Delta ubiG$ strains (data not shown), and was also
131 unable to suppress the growth phenotype of $\Delta ubiH\Delta ubiA$ or $\Delta ubiH\Delta ubiD$ mutants (Figure
132 1B), showing that UbiUV intervene specifically at the hydroxylation steps and otherwise
133 depend upon all the other components of the aerobic UQ biosynthesis pathway to do so.
134 These results indicate that in the presence of O₂, expression of UbiUV can substitute for the
135 O₂-dependent UbiIHF hydroxylases and that integrity of the UbiU [Fe-S] cluster is required.

136 Remarkably, expression of the pES154 plasmid was also able to suppress growth
137 defects of the $\Delta ubiJ$ mutant (Figure 2A). UbiJ is an auxiliary factor important for organizing
138 the aerobic Ubi metabolon. We reasoned that suppression was made possible thanks to the

139 presence of the chromosomally encoded UbiT that shares sequence similarity with UbiJ. To
140 test this, we repeated the complementation test in two new strains, $\Delta ubiH\Delta ubiJ$ and
141 $\Delta ubiH\Delta ubiT$. The pES154 plasmid still complemented growth defects of the $\Delta ubiH\Delta ubiJ$
142 mutant, but it was unable to complement the $\Delta ubiH\Delta ubiT$ mutant (Figure 2B). Similarly,
143 pES154 was found to suppress the growth defect phenotype of a $\Delta ubiF\Delta ubiJ$ mutant but not
144 a $\Delta ubiF\Delta ubiT$ mutant (Figure 2C). These results showed that in the presence of O₂, increased
145 dosage of *ubiUV* genes suppresses the lack of O₂-dependent hydroxylases UbiF and UbiH in
146 an UbiT-dependent/UbiJ-independent manner.

147 To confirm that phenotypic suppression was due to UQ₈ synthesis, we quantified the
148 UQ₈ content by HPLC analysis coupled to electrochemical detection (ECD) for all strains
149 described above (Figure 3A). Results showed that mutant strains lacking UbiI-UbiK, UbiH
150 and/or UbiF were severely deficient in UQ. The pES154 plasmid enabled $\Delta ubiH$, $\Delta ubiF$, or
151 $\Delta ubiIH$ strains to synthesize 30-50% of the UQ level of the wild-type (wt) strain (Figure 3A, 1st
152 panel). The levels of UQ obtained in the $\Delta ubiIH\Delta ubiF$ and $\Delta ubiIK$ mutant strains with the
153 pES154 plasmid were much lower. We stress that the UQ levels cannot be directly correlated
154 with the phenotypic analysis (Figures 1-2) since culture media were different (LB vs M9
155 succinate) to allow recovery of enough biological material for the HPLC-ECD analyses.
156 Importantly, the pBAD-*ubiU(C176A)V* plasmid was unable to promote UQ synthesis in $\Delta ubiH$
157 (Figure 3A, 2nd panel). Last, UQ₈ content assay confirmed that UbiT, but not UbiJ, was
158 necessary for UbiUV to synthesize UQ in aerobic conditions (Figure 3A, 3rd panel).

159 The results above showed that UbiUV hydroxylate UQ precursors, when expressed
160 under aerobic conditions. This result raised the possibility that under such conditions, O₂
161 might be used as a co-substrate of the hydroxylation reactions, as is the case for UbiI, UbiH
162 and UbiF in wt cells (5). To test this hypothesis, we exposed cells to ¹⁸O₂ and monitored the
163 labelling of UQ by HPLC-ECD-MS. Two hours after ¹⁸O₂ addition, the level of UQ₈ increased in
164 both strains (Figure 3B). Before adding ¹⁸O₂, the mass spectra of UQ synthesized by wt or
165 $\Delta ubiIH\Delta ubiF$ cells containing pES154 displayed H⁺ and NH₄⁺ adducts with m/z ratio
166 characteristic of unlabeled UQ (Figure 3C and D). As expected, two hours after adding ¹⁸O₂,
167 most of the UQ₈ pool in wt cells contained three ¹⁸O₂ atoms (Figure 3E), in agreement with
168 O₂ being the co-substrate of the aerobic hydroxylation steps (5). In contrast, we detected
169 only unlabeled UQ₈ in the $\Delta ubiIH\Delta ubiF$ strain expressing UbiUV (Figure 3F), demonstrating

170 that UbiUV utilize another oxygen donor than O₂, even when operating under aerobic
171 conditions.

172 Altogether, both phenotypic and UQ₈ quantification results allowed us to conclude
173 that UbiU and UbiV, when produced in sufficiently high-level, function in the canonical
174 “aerobic” UQ₈ biosynthesis pathway by catalyzing [Fe-S]-dependent hydroxylation of the
175 benzene ring in an O₂-independent reaction. Remarkably, UbiT is necessary for such aerobic
176 UbiUV-mediated synthesis to occur and cannot be substituted by UbiJ.

177

178 **2. The ISC [Fe-S] biogenesis machinery is required for anaerobic UQ biosynthesis**

179 The UbiU and UbiV proteins each contain a [4Fe-4S] cluster, which is essential to the
180 synthesis of UQ in anaerobic conditions (3). Assembly of [4Fe-4S] clusters requires complex
181 biosynthetic machineries, ISC and SUF (15). Therefore, the UQ₈ levels were monitored in Δ *isc*
182 and Δ *suf* mutants grown in anaerobic conditions (Figure S3). In addition to UQ₈, the
183 quantification of DMK₈ and MK₈ was also performed. UQ₈ content in Δ *isc* mutants was
184 strongly impaired (around 15% of the wt), and was much less affected in Δ *suf* mutants (60-
185 80% of the wt). DMK and MK content remained mostly unaltered. Collectively, these results
186 showed that ISC and SUF systems are not involved in DMK and MK biosynthesis and that the
187 ISC system is the most relevant in UQ₈ biosynthesis likely through the maturation of [4Fe-4S]
188 clusters in UbiU and UbiV.

189

190 **3. Anaerobic and micro-aerobic UQ biosynthesis**

191 Genome scale studies have predicted that *ubiUV* genes are under the control of the
192 anaerobic Fnr transcriptional activator (16, 17). In contrast, *ubiT* did not appear as a
193 potential Fnr target. This prompted us to investigate the effect of anaerobiosis (0% O₂),
194 microaerobiosis (0.1% O₂), and aerobiosis (21% O₂) on the level of UbiU, UbiV, and UbiT
195 proteins. In order to follow the quantity of UbiTUV proteins in physiological conditions, we
196 constructed a series of recombinant strains producing the UbiT, UbiU, or UbiV proteins with
197 a C-terminal SPA tag (18) encoded from a gene fusion at their chromosomal loci. We
198 examined protein production by Western Blot assay using an anti-flag antibody and assessed
199 loading with a polyclonal antibody against YbgF (CpoB). All three UbiTUV-SPA tagged
200 proteins were present in strains grown in anaerobiosis (Figure 4A) and microaerobiosis
201 (Figure 4B). In aerobiosis, production of UbiU and UbiV was no longer observed whereas a

202 significant level of UbiT was still visible. The contribution of Fnr to anaerobiosis- or
203 microaerobiosis-mediated activation of *ubiU* and *ubiV* genes was confirmed as no cognate
204 UbiU or UbiV associated band was observed in a Δfnr mutant (Figure 4A-B). Interestingly,
205 UbiT level was also reduced in the Δfnr mutant in $-O_2$. Last, in order to validate the
206 physiological significance of the Fnr regulatory circuit depicted above, we quantified the
207 amount of UQ₈ produced in wt and Δfnr strains, during aerobiosis and anaerobiosis (Figure
208 4C). In comparison to the UQ content found in the wt strain in aerobiosis, the level in
209 anaerobiosis was reduced by half. Importantly, we observed that almost no UQ was
210 detected in the Δfnr mutant (Figure 4C). This revealed the pivotal role that Fnr plays in
211 allowing UQ₈ synthesis in the absence of O₂.

212

213 **4. Genetic control of *ubiUVT* gene expression**

214 Previous genome Chip-seq analysis reported binding of Fnr within the *ubiT-ubiUV* intergenic
215 region. Additionally, in a whole genome sequence search study, one transcription start site
216 has been described upstream of the *ubiUV* operon (*ubiUV_p*) and two sites described
217 upstream of *ubiT* (*ubiT_{p1}*, *ubiT_{p2}*) (19) (Figure 5A, 5B). Upon inspection of that region, we
218 were able to identify two potential Fnr binding sites fitting well with the described Fnr
219 binding consensus. The F1 site, reading TTGATTTAAGGCAG is located 36 nucleotides (nt)
220 upstream the *ubiUV_p* transcription start site (Figure 5A). The F2 site, reading
221 TTGATTATACCGC locates 33 nt upstream the proximal +1 transcription starting site *ubiT_{p2}*
222 and 19 nt downstream the distal *ubiT_{p1}* (Figure 5A, 5B).

223 To detail the molecular mechanism of regulation and to dissect the promoter
224 organization of the intergenic region between *ubiUV* and *ubiT*, we used transcriptional
225 fusions with GFP (20). We used 4 different transcriptional fusions encompassing *ubiUV_p*,
226 *ubiT_{p1}*, *ubiT_{p2}*, and a construction *ubiT_{p1p2}* containing the two promoters of *ubiT* (Figure 5B).
227 We compared the expression of these transcriptional fusions in anaerobiosis, in a Δfnr
228 mutant complemented or not with a pBAD-*fnr* plasmid. The *ubiUV_p* and *ubiT_{p2}* promoters
229 were strongly activated in the presence of pBAD-*fnr*, whereas the *ubiT_{p1}* promoter was not
230 (Figure 5C-D). This suggested that the *ubiUV_p* promoter was activated by Fnr binding to the
231 F1 site, and that the *ubiT_{p2}* promoter was activated by Fnr binding to the F2 site. When we
232 introduced mutations in the F1 binding site (5 mutated nucleotides; mutF1; Figure 5A), the
233 activation of the expression from the *ubiUV_p* transcriptional fusion was severely reduced

234 (Figure 5C). Mutations of the F2 site (*mut* Δ F2 complete deletion or *mut*F2 with 5 mutated
235 nucleotides; Figure 5A) also affected the expression of the *ubiT*_{p1p2} transcriptional fusion, but
236 a basal level of expression was maintained, probably due to the expression from the distal
237 *ubiT*_{p1} promoter (Figure 5E).

238 Next, we introduced the same mutations in the F1 and F2 Fnr binding sites at the
239 locus in the *ubiU-ubiT* intergenic region in the chromosome of the strains producing UbiV-
240 SPA or UbiT-SPA tagged proteins. Mutation within the F1 site upstream *ubiU* completely
241 prevented the production of UbiV in the absence of O₂ (Figure 5F). Mutation within the F2
242 site upstream the proximal *ubiT*_{p2} promoter prevented the induction of *ubiT* in the absence
243 of O₂, without altering the basal level of UbiT-SPA observed in the presence of O₂ (Figure 5F
244 and Figure S4). Notably, the mutation in the F1 binding site did not affect the expression of
245 *ubiT* and conversely, mutation of the F2 binding site did not affect the expression of *ubiV*.

246 Altogether, these results showed that Fnr activates *ubiUV* transcription under
247 anaerobiosis, while *ubiT* expression can be triggered from two promoters, one aerobically
248 active (P1) and the other anaerobically active (P2) under Fnr control.

249

250 **5. Physiological role of UbiUVT at different O₂ levels**

251 We have previously reported that UbiU, UbiV, and UbiT are essential for anaerobic synthesis
252 of UQ in *E. coli* when grown in LB, glycerol/DMSO, or lactate/NO₃⁻ (3). However, the
253 contribution to *E. coli* physiology of UQ synthesized by UbiUVT in anaerobic conditions was
254 not investigated in detail. We made use of a set of mutants altered in aerobic (*ubiH*) or
255 anaerobic (*ubiUV*, *ubiT*) UQ₈ synthesis, as well as mutants altered in DMK/MK biosynthesis
256 (*menA*) to assess the contribution of each type of quinone for growth in a wide range of O₂
257 level, 21% (aerobic), 0.1% (microaerobic), and 0% O₂ (anaerobic), and with varying carbon
258 sources (e.g. glycerol or glucose) and electron terminal acceptors (e.g. O₂ or NO₃⁻).

259 In the presence of glycerol and NO₃⁻ under aerobic conditions (Figure 6, upper left
260 panel) Δ *ubiUV* and Δ *ubiT* strains showed no growth phenotype. In such conditions, while
261 NO₃ is present, O₂ is used for respiration. This contrasted with the Δ *ubiH* mutant, which was
262 severely affected. Combining Δ *ubiH* and Δ *ubiUV* bore no aggravating effect. In contrast,
263 combining both Δ *ubiH* and Δ *menA* had an aggravating effect, indicating that in addition to
264 UQ, DMK and/or MK can support *E. coli* growth even in aerobiosis, as previously suggested

265 (21). In microaerobic conditions (Figure 6, upper center panel), no phenotype was observed
266 for $\Delta ubiUV$ or $\Delta ubiT$ strains. In contrast, the $\Delta menA \Delta ubiH$ strain still exhibited a clear
267 defect, suggesting that *ubiUV* and *ubiT* do not bear a prominent role in NO_3^- -dependent
268 respiratory metabolism under microaerobic conditions, despite being expressed in
269 microaerobiosis (see above). This notion was also supported by the fact that at 0.1% O_2 , the
270 $\Delta ubiH$ and $\Delta ubiH \Delta ubiUV$ strains did not show any phenotype. At 0.1% O_2 , UQ-dependent
271 metabolism through cytochrome *bd* or *bo* oxidases would remain inconsequential and cells
272 presumably rely on DMK/MK-dependent metabolism for anaerobic respiration (22). Last, in
273 anaerobic conditions, with NO_3^- used for respiration, $\Delta ubiUV$, $\Delta ubiT$ and $\Delta menA$ strains
274 showed wt-like growth phenotype (Figure 6, upper right panel). However, combining $\Delta menA$
275 and $\Delta ubiUV$ mutations or $\Delta menA$ and $\Delta ubiT$ mutations drastically hampered NO_3^-
276 respiratory capacities. In fact, growth of these mutants on M9 glycerol NO_3^- was barely
277 better than a Δfnr strain (Figure 6), which was used as control since it was shown that such
278 strain is unable to respire nitrate but can still use glucose anaerobically (23). These results
279 indicated that anaerobically UbiUVT-synthesized UQ and MK are fully interchangeable
280 electron carriers during NO_3^- respiration under full anaerobiosis (24). Furthermore, we could
281 exclude that the aerobic UQ biosynthetic pathway could contribute to growth in such
282 conditions as the $\Delta ubiH$ and $\Delta menA \Delta ubiH$ mutants exhibited no growth phenotype.

283 In the presence of glucose as a carbon source and under aerobiosis, $\Delta ubiUV$ and
284 $\Delta ubiT$ mutants exhibited wt-like growth capacity (Figure 6, left middle panel). The $\Delta ubiH$
285 mutant showed some slower growth but a most spectacular negative additive effect was
286 observed upon combining $\Delta ubiH$ and $\Delta menA$ mutations. It likely points out a role for
287 DMK/MK in aerobic electron transport (25). In anaerobiosis, neither $\Delta ubiH$ nor $\Delta menA$, alone
288 or in combination, showed defect in the presence of glucose as a carbon source (Figure 6,
289 middle right panel). In contrast, $\Delta menA \Delta ubiUV$ or $\Delta menA \Delta ubiT$ mutants exhibited additive
290 growth defect (Figure 6, middle right panel). This indicated that the UbiUVT-biosynthesized
291 UQ was crucial for growth in glucose fermentative conditions, in the absence of MK. A
292 possibility was that this negative effect reflected auxotrophy for uracil, whose synthesis
293 depends upon electron transfer from PyrD dihydroorotate dehydrogenase to fumarate
294 reductase (FrdABCD) via quinones in anaerobiosis (26). As a matter of fact, adding uracil to
295 the medium had a rescuing effect (Figure 6, lower right panel), supporting the notion that

296 uracil deficiency was responsible for the growth defect observed in the *ΔubiUV ΔmenA*
297 mutant in anaerobiosis. This was an important observation as early studies had proposed
298 that the PyrD/FrdABCD electron transfer chain relied mostly on MK/DMK and marginally, if
299 at all, on UQ (26). Our observation clearly shows that anaerobically synthesized UQ can also
300 allow functioning of PyrD. Incidentally, we noticed that the addition of uracil did not rescue
301 the growth defect of the *ΔmenAΔubiH* mutant in aerobiosis, but we have no explanation for
302 this observation.

303

304 **6. Contribution of the O₂-independent UQ biosynthesis pathway to mouse intestine** 305 **colonization**

306 Since enterobacteria evolve mostly in anaerobic conditions in their natural habitat, we
307 evaluated the physiological importance of the O₂-independent UQ biosynthesis pathway in
308 the mouse intestine. To do so, we performed competition experiments between two
309 isogenic strains, MP7 and MP13, which respectively express mCherry and GFP in the
310 presence of tetracycline (27). We deleted *ubiUV* in the MP13 background and confirmed, as
311 expected, that this strain was deficient for UQ₈ when grown anaerobically (Figure S5A). MK
312 was previously shown to be important for efficient colonization of the mouse intestine by *E.*
313 *coli* (28). Thus, we also constructed a *ΔmenA* mutant in the MP13 background. We checked
314 that deletion of *ΔmenA* abrogated the synthesis of DMK and MK (Figure S5B and C). The
315 fitness of the *ΔubiUV* and *ΔmenA* mutants was tested in competition experiments with the
316 MP7 wt strain. We monitored the abundance of each strain in the feces of mice up to 10
317 days after co-inoculation by oral gavage (Figure 7A). In both experiments, the total CFU
318 count reached $\sim 10^8$ per gram of feces 24 hours post inoculation (Figure 7B and C and S6A
319 and B) and then gradually decreased to $\sim 10^5$, showing efficient colonization of the MP7
320 strain. The abundance of the *ubiUV* mutant was slightly decreased compared to wt (Figure
321 7B and S6A), which translated in an average competitive index (CI) <1 (Figure 7D and S6C) at
322 days 1, 2, 4, and 10. We noticed however a rather high inter-individual variability (Figure
323 S6C). In contrast, the *ΔmenA* mutant was markedly less abundant than the wt (Figure 7C and
324 S6B) and was even undetectable at day 10. CI <1 were observed for every mouse at every
325 sampling (Figure 7E and S6D) and the values obtained were much lower than in the case of
326 the *ΔubiUV* mutant. Collectively, these data confirm that DMK/MK is the most important
327 quinone for the physiology of *E. coli* in the mouse intestine (28). However, they also reveal a

328 contribution, albeit minor, of the O₂-independent UbiUV-mediated UQ biosynthesis
329 pathway.

330

331 **7. Role of UbiT within the anaerobiosis-aerobiosis shift**

332 Phenotypic analysis above revealed that anaerobically UbiUVT-synthesized UQ was
333 contributing to growth via glucose fermentation or NO₃⁻ respiration. In both conditions,
334 anaerobic UbiUVT-synthesized UQ was functionally redundant with anaerobically
335 synthesized DMK/MK. Because UQ is crucial under aerobiosis, we reasoned that
336 anaerobically synthesized UQ might prepare the cells to adapt to an aerobic environment,
337 i.e. before the aerobic UbiIHF-dependent synthesis takes over. Thus, we investigated the
338 role of UbiUVT-synthesized UQ in the anaerobiosis-aerobiosis transition.

339 Firstly, we used $\Delta menA\Delta ubiH$ and $\Delta menA\Delta ubiUV$ strains that only produce UQ under
340 anaerobiosis and aerobiosis, respectively. Strains were grown in LB supplemented with NO₃⁻
341 under anaerobic conditions for 24 hours, then switched to aerobic conditions with succinate
342 as carbon source, i.e. in conditions wherein growth strictly relies on UQ (24). The wt, $\Delta menA$,
343 and the $\Delta menA\Delta ubiUV$ strains showed differential efficiency in shifting from anaerobiosis to
344 aerobiosis, the lag periods lasting 2 to 4 hours for the wt and $\Delta menA$ strains, and lasting 7
345 hours for the $\Delta menA\Delta ubiUV$ mutant (Figure 8A). This indicated that UbiUV-synthesized UQ
346 was important for allowing a fast transition, presumably as a consequence of a higher level
347 of UQ in wt than in $\Delta menA\Delta ubiUV$ mutant. Eventually, both strains showed the same growth
348 rate in exponential phase and reached the same final OD₆₀₀ value, suggesting that the
349 UbiIHF-synthesized UQ was activated and fully compensated the requirement of UQ in
350 extended aerobic conditions. To confirm this hypothesis, we re-inoculated these cells into
351 the same medium (Figure 8A, refresh), and as expected we observed that lag periods were
352 the same for both strains since they had accumulated the same level of UQ since the
353 beginning of the growth. In contrast, the $\Delta menA\Delta ubiH$ mutant – a strain defective for the
354 aerobic UQ-synthesis pathway – exhibited drastic differences as compared with the two
355 strains above, i.e. a slower and shorter exponential phase and a lower final OD₆₀₀ value.
356 Moreover, $\Delta menA \Delta ubiH$ mutant failed to resume growth upon reinoculation in fresh
357 medium (Figure 8A). Altogether these results indicated that the level of anaerobically UbiUV-
358 synthesized UQ sustained the anaerobic-to-aerobic shift but failed to sustain protracted
359 aerobic growth. This view was further supported by measuring the UQ content during

360 transition from anaerobic to aerobic conditions in a separate experiment (Figure 8B). For
361 this, cultures in LB of $\Delta ubiUV$ or $\Delta ubiT$ mutants were subjected or not to chloramphenicol
362 (Clp) treatment prior to shift and samples were taken at 0 min, 30 min, and 120 min for UQ
363 quantification. UQ level increased with time in both the wt and the $\Delta ubiUV$ mutant but in
364 the 30-120 min period it stopped increasing in the presence of translation inhibitor Clp. The
365 likeliest explanation is that UQ biosynthesis is driven by UbiUV before the shift and later de
366 novo synthesized by UbiH/F in aerobic conditions. This suggested that the 3 hydroxylases
367 UbiL, H, and F were already present under anaerobiosis, in a stand-by state, waiting for O₂ to
368 allow hydroxylation. Importantly, this was confirmed as levels of UbiL, H, and F proteins were
369 found to be similar in both aerobic and anaerobic conditions (Figure S7).

370 Secondly, the role of the accessory factor, UbiT, was investigated using the $\Delta menA$
371 $\Delta ubiT$ mutant. As described before, the $\Delta menA\Delta ubiT$ strain was grown first in LB with NO₃
372 under anaerobiosis, subsequently shifted in succinate minimal medium, and growth was
373 monitored. A most unexpected and spectacular effect was observed as lag period with this
374 strain was 3 and 5 times longer than the one observed for the $\Delta menA \Delta ubiUV$ and wt strains,
375 respectively (Figure 8A). However, the $\Delta menA\Delta ubiT$ strain finally reached a final OD₆₀₀ value
376 similar to WT, $\Delta menA$, $\Delta menA \Delta ubiUV$ strains at 40h, and also resumed growth upon re-
377 inoculation at 40h (Figure 8A). This highlighted a crucial role of UbiT in the anaerobic-
378 aerobic transition phase. This result was strengthened by direct quantification of UQ
379 synthesized with time after shifting cultures from anaerobiosis to aerobiosis (Figure 8B). The
380 $\Delta ubiT$ mutant exhibited a 2-fold reduction in UQ as compared with the $\Delta ubiUV$ mutant after
381 the shift. When Clp was added, the difference was much smaller. This confirmed that UbiT is
382 necessary at the onset of aerobic UQ biosynthesis, presumably via the UbiH/F complex.

383

384 **8. The *yhbS* gene is not involved in UQ-based metabolism**

385 The *yhbS* gene predicted to encode an acetyltransferase, lies downstream the *ubiT* gene
386 (Figure S8A). It was recently proposed to intervene in sncRNA-mediated expression control
387 (29). Using RT-PCR, we showed that *yhbS* and *ubiT* genes share a single transcription unit
388 (Figure S8B). Using YhbS-SPA tag protein, we observed that YhbS protein synthesis takes
389 place both under aerobiosis and anaerobiosis. The level of YhbS-SPA protein appears slightly
390 higher in -O₂ and this induction seems to be lost in the Δfnr mutant, as expected if *yhbS* and
391 *ubiT* genes are co-expressed and co-regulated by Fnr (Figure S8C). The $\Delta yhbS$ mutant shows

392 no defect in NO_3^- respiratory capacity, and no aggravating effect was observed upon
393 combining $\Delta yhbS$ and $\Delta menA$ mutations (Figure S8D). Last, we carried out shift experiments,
394 from $-\text{O}_2$ to $+\text{O}_2$, as described above for *ubiT* and failed to identify any defect in the $\Delta yhbS$
395 mutant (not shown). Altogether with previous assays failing to reveal a defect in UQ levels in
396 anaerobiosis in the $\Delta yhbS$ mutant (3), these results allowed us to rule out a role of YhbS in
397 UQ synthesis.
398

399 **CONCLUSION**

400

401 UQ is an essential component of electron transfer chains, and of respiratory metabolism. For
402 decades, the dogma has been that UQ was exclusively used for aerobic respiratory
403 metabolism, whereas DMK/MK was used for electron transfer in anaerobic respiratory
404 chains. Following our recent discovery that UQ is also synthesized under anaerobiosis, which
405 contradicted the above assumption (3), the present study identified two versatile anaerobic
406 physiological processes that rely on the anaerobic UQ biosynthesis pathway, namely NO_3^-
407 respiration and uracil biosynthesis. Moreover, we provide clear evidence that UbiUV
408 catalyze hydroxylation steps independently from O_2 . Last, UbiT was found to play a key role
409 in both anaerobiosis and aerobiosis conditions, allowing a smooth transition between the
410 two conditions. Overall, this analysis uncovers a new facet of the strategy used by *E. coli* to
411 adapt to changes in O_2 level and respiratory conditions. This is of particular interest in the
412 context of gut microbiota studies, as changes in O_2 level and in respiratory electron
413 acceptors are key factors that the host uses to select the type of flora present through the
414 different sections of the intestine (30).

415 UbiUV-mediated UQ synthesis takes place under anaerobiosis. Here we showed that
416 this is made possible by Fnr-mediated activation of expression of the *ubiUV* operon that
417 takes place from microaerobiosis (0.1% O_2) to anaerobiosis. In contrast, expression of the
418 *ubiT* gene is more versatile with 2 promoters, one under Fnr control, allowing UbiT synthesis
419 under micro- and an-aerobiosis, simultaneously with UbiUV, and the second constitutive
420 one, insuring expression in aerobiosis. This genetic regulation is consistent with the presence
421 of UbiT proteins under both aerobic and anaerobic conditions. Such a versatile expression
422 meets with other evidence we collected, which together pave the way to an important role
423 of UbiT in anaerobiosis to aerobiosis transition: (i) UbiT is required for insuring continuous
424 UQ synthesis upon shifting from anaerobiosis to aerobiosis, (ii) *ubiT* was found to
425 compensate for the lack of *ubiJ* in conditions where high dosage of *ubiUV* genes suppressed
426 absence of *ubiIHF* under aerobiosis, (iii) UbiIHF enzymes are present in anaerobiosis but not
427 active as one would expect for O_2 -dependent hydroxylases. This indicates that the O_2 -
428 dependent pathway is in a stand-by mode in anaerobic conditions, waiting only for the
429 presence of O_2 to activate the O_2 -dependent hydroxylases and produce UQ, as proposed

430 previously (31). This is also consistent with the fact that UbiUV synthesis is strictly controlled
431 at the transcriptional level, whereas expression of *ubiIHF* is constitutive. Altogether, this
432 leads us to propose that UbiT and UbiJ are required for the formation of two related but
433 distinct metabolons, respectively an anaerobic one containing UbiUV, and an aerobic one
434 containing UbiIHF. Besides, both UbiJ and UbiT are likely to bind UQ biosynthetic
435 intermediates via their SCP2 domain, thereby providing the substrates to UbiUV and UbiIHF
436 (9, 32).

437 UbiUV catalyze hydroxylation of the benzene ring in the absence of O₂. Moreover,
438 our results show that they can substitute to aerobic hydroxylases UbiIHF in the presence of
439 O₂, but that they still catalyze the hydroxylation without relying on O₂ in this condition. This
440 raises the question of the source of the O atom under anaerobiosis. Previous analysis on
441 RhlA, a member of the U32 protein family to which UbiU and V belong, indicated that
442 prephenate, an intermediate within the aromatic amino acid biosynthesis pathway, could
443 act as O donor (11). Our ongoing studies aim at investigating such a possibility in the case of
444 anaerobic UQ biosynthesis. [Fe-S] clusters seem to play a role in the process, since *isc*
445 mutants devoid of anaerobic [Fe-S] biogenesis machinery and UbiU variant lacking [Fe-S]
446 cluster fail to produce UQ. The simplest hypothesis is that [Fe-S] clusters are transferring
447 electrons from the O source to a terminal reductase, both to be identified.

448 UbiUVT-synthesized UQ has a significant contribution to growth in anaerobiosis and
449 in microaerobiosis (0.1% O₂). Indeed, we found that UbiUVT-synthesized UQ are key for NO₃⁻
450 respiration in the absence of (D)MK, in agreement with early biochemical work on formate-
451 nitrate reductase (26) and with our previous study reporting that *Pseudomonas aeruginosa*
452 denitrifying activity depends on UbiUVT synthesized UQ (32). Moreover, we observed that
453 the anaerobically synthesized UQ greatly contributes to uracil synthesis. This was
454 unexpected as uracil synthesis was reported to depend mainly on the oxidation of (S)-
455 dihydroorotate to orotate with fumarate as hydrogen acceptor and DMK/MK as an electron
456 carrier (26). Our present physiological studies demonstrate that the anaerobically produced
457 UQ can fully compensate the DMK/MK loss, likely through an as yet unknown reductase
458 since UQ is too electro-positive to be a FrdABCD substrate (33). Last, UQ could be used as an
459 electron sink to other catabolic processes taking place in both aerobiosis and anaerobiosis

460 such as heme biosynthesis, wherein HemG enzyme utilizes UQ or MK for the conversion of
461 protoporphyrinogen IX into protoporphyrin IX (34).

462 The contribution of anaerobically synthesized UQ for *E. coli* multiplication in the gut
463 appeared as marginal. This implies that either absence of UV-synthesized UQ was masked by
464 MK/DMK synthesis, or anaerobic UQ-dependent processes such as NO_3^- respiration or uracil
465 biosynthesis is dispensable. Clearly the first possibility is the likeliest given the paramount
466 importance of anaerobic respiration for *E. coli* multiplication in the gut (35, 36), as nicely
467 confirmed by the drastically altered multiplication of MK/DMK deficient cells (Figure 7). This
468 is of particular interest as presence and nature of respiratory electron acceptors were
469 proposed to be drivers of bacterial community composition in the different regions of the
470 intestine (30). Likewise, the relatively high O_2 level in duodenum, of NO_3^- in ileum, and
471 hypoxia in cecum were proposed to be causal of the different flora hosted in these regions in
472 healthy host. Strategies used by *E. coli* to live in such different respiratory and fermentative
473 conditions are therefore key aspects of its adaptation to the host. In this context, it is
474 important to understand the mechanism underlying the switch from O_2 -rich to NO_3^- -rich
475 and/or hypoxic compartments and the present study highlights the added value of having
476 overlapping systems permitting smooth shift from anaerobic NO_3^- to aerobic respiration.

477

478 **MATERIAL AND METHODS**

479

480 **Strain constructions (Table 1)**

481 Most knockout strains were obtained by generalized Φ P1 transduction using donor strains
482 from the Keio collection (37). For introducing the SPA-tag on the chromosome or for
483 generation of specific knockouts, PCR recombination with the lambdaRed system was used,
484 using the oligonucleotides indicated in Table 1 (18, 38). When necessary, the antibiotic
485 resistance marker was removed using FLP recombinase expression from plasmid pCP20 as
486 described previously (39). Cassette removal and plasmid loss were verified by antibiotic
487 sensitivity and confirmed by PCR amplification. Point mutations were introduced on the
488 chromosome using the pKO3 vector (40).

489 For mouse intestine colonization experiments, we used MP7 and MP13 strains, which
490 derive from the commensal *E. coli* MP1 strain (27). MP7 and MP13 express respectively
491 mCherry or GFP under the control of a tetracycline inducible promoter. $\Delta menA$ and $\Delta ubiUV$
492 deletions were introduced in MP13 using generalized Φ P1 transduction.

493

494 **Plasmid constructions (Table 2)**

495 pUA66 and pUA-*ubiUV*p plasmids were obtained from the library of *E. coli* promoters fused
496 to GFP coding sequence (20). The *ubiT* transcriptional fusions were constructed using
497 primers indicated in Table 3 and cloned in XhoI/BamHI sites of pUA66. Expression plasmids
498 for *ubiUV* and *fnr* were constructed using primers indicated in Table 3 and cloned in
499 EcoRI/SalI sites of pBAD24 vector (41). Expression plasmids for *ubiIHF* and *ubiM_Neisseria*
500 genes were constructed using primers indicated in Table 3 and cloned in EcoRI/XhoI sites of
501 pTet vector. A region of 1275 base pairs encompassing *ubiU* and *ubiT* promoters was cloned
502 in pKO3 vector (40). Mutations were introduced in the pKO3-*ubiTU* vector, in the pBAD-
503 *ubiUV*, and in the transcriptional fusions by PCR mutagenesis on plasmid, using the
504 oligonucleotides indicated (Tables 2 and 3).

505

506 **Media and growth conditions**

507 Strains were grown in LB miller (10g/l of tryptone, 10g/l of NaCl and 5g/l of yeast extract) or
508 M9 medium (6 g/l $\text{Na}_2\text{HPO}_4 \cdot 7\text{H}_2\text{O}$, 3 g/l KH_2PO_4 , 0.5 g/l NaCl, 1 g NH_4Cl , 2 mM MgSO_4 ,
509 1mg/ml thiamine) supplemented with 0.2% glucose, 0.2% glycerol, or 50mM succinate as
510 the carbon source. For anaerobic cultures, media were degazed and incubated in anaerobic
511 environment for at least 24 hours prior to use, if necessary supplemented with 25mM KNO_3
512 as electron acceptor and uracil 25ug/ml or casamino acids at 0.05%.

513 For microaerobic experiments, media and plates were pre-equilibrated and cells were
514 cultured in a Whitley® H35 hypoxic station with 95% N_2 , 5% CO_2 and the desired O_2
515 concentration. Humidity and temperature were set up at 85% and 37°C, respectively. For
516 anaerobic-aerobic shift experiments, all anaerobic steps were performed in a JACOMEX®
517 Campus anaerobic chamber under N_2 atmosphere at 1ppm O_2 maximum. Cells were first
518 isolated anaerobically in LB agar plates supplemented with 0.2% Glucose and incubated
519 overnight at 37°C. Next day, cells were cultured anaerobically in 3mL LB supplemented with
520 25mM NO_3^- for 24 hours at 37°C. Still under anaerobiosis, cells were collected by
521 centrifugation, supernatant was discarded, and pellets were washed twice using 1mL M9
522 medium without carbon source and normalized at 0.1 OD units in M9 medium
523 supplemented with 50mM Sodium Succinate. At this point, cultures were moved out to
524 atmospheric air and growth was followed by triplicate at 37°C on 200µl of culture in a 96-
525 well plate using a TECAN infinite M200 plate reader. At 40h of culture, cells were diluted
526 1/20 in new M9 50mM Sodium Succinate medium and readings were resumed until 60
527 hours.

528 Aerobic and anaerobic cultures for quinone analysis:

529 For aerobic cultures, 5 mL of LB medium, supplemented with Ampicillin (100 µg/mL) and
530 0.05% arabinose when necessary to induce the expression from the pBAD vectors, was
531 inoculated with 100 µl of an overnight culture in glass tubes (15 cm long and 2 cm in
532 diameter) and incubated at 37°C, 180 rpm overnight.

533 Anaerobic cultures were performed in Hungate tubes as previously described (3). Briefly, LB
534 medium was supplemented with 100 mM KNO_3 as final electron acceptor, 100 mg/liter L-
535 cysteine (adjusted to pH 6 with NaOH) in order to reduce residual molecular oxygen and 2.5
536 mg/liter reasazurin. This medium was distributed in Hungate tubes and deoxygenated by

537 high purity argon bubbling for 40 min. The Hungate tubes were sealed and autoclaved. The
538 resazurin was initially purple, it turned to pink after deoxygenation and become colorless
539 after autoclave. The preculture was performed overnight at 37°C in Eppendorf tubes filled to
540 the top with LB medium containing 100 mM KNO₃. The Hungate tubes were then inoculated
541 through the septum by disposable syringes and needles with 100 µL of precultures and
542 incubated at 37°C without agitation. The resazurin remained colorless during culture
543 indicating anaerobic conditions.

544 For anaerobic to aerobic shift assay, MG1655 WT, *ΔubiUV*, and *ΔubiT* strains were grown
545 anaerobically in Hungate tubes for ~ 4 hours. Then, 26 µL of chloramphenicol (200 µg/mL)
546 was injected through the septum by Hamilton syringe. After 20 minutes, the Hungate tubes
547 were unsealed, 2 mL of cultures was taken for lipid extraction and quinone analysis. The rest
548 of cultures was transferred to 250 mL Erlenmeyer flasks and placed at 37°C, 180 rpm for 2
549 hours. 2 mL aliquots of cultures were taken at 30 min and 120 min after transition to
550 ambient air for lipid extraction and quinone analysis.

551

552 **SDS-PAGE and Western blotting**

553 Total cell extracts were prepared by resuspending cell pellets in Laemli buffer 1X at a
554 concentration of 0.3 OD_{600nm} units in 10 µl, and then heating for 10 minutes at 95°C. After
555 separation of 8 µl of total cell extracts on SDS-PAGE, electrotransfer onto nitrocellulose
556 membranes was performed using Trans-Blot turbo transfer system from Biorad. After
557 blocking in PBS 1X + milk 5%, SPA-tagged proteins were detected with monoclonal anti-Flag
558 M2 antibody purchased from Sigma. YbgF protein was used as an internal control and
559 revealed with polyclonal anti-YbgF antibodies. Fluorescent secondary antibodies were
560 respectively IRDye 800 anti-mouse and IRDye 680 anti-rabbit purchased from Li-Cor.
561 Scanning and quantification were performed on a Li-Cor Odyssey-Fc imaging system, reading
562 at 700 nm (for YbgF detection) or 800 nm (for Flag detection).

563

564 **Transcriptional fusions with GFP**

565 We used several clones from the *E. coli* transcriptional fusions library (20) and we
566 constructed the required additional transcriptional fusions (see above for plasmid
567 construction and Table 2). *Δfnr E. coli* strain was co-transformed with plasmids carrying the

568 *gfp* transcriptional fusions and compatible pBAD24 or pBAD-*fnr* plasmids. Selection plates
569 were incubated at 37°C for 16h. 600 µl of LB medium supplemented with kanamycin and
570 ampicillin, and with 0.02% arabinose for pBAD-driven expression, were incubated (4
571 biological replicates for each assay) and grown for 16 hours at 37°C in 96-well polypropylene
572 plates of 2.2 ml wells in anaerobiosis. Cells were pelleted and resuspended in PBS
573 supplemented with 30 µg/ml chloramphenicol and incubated at 4°C for 1 hour before
574 fluorescent intensity measurement was performed in a TECAN infinite M200 plate reader.
575 150 µl of each well was transferred into black Greiner 96-well plate for reading optical
576 density at 600nm and fluorescence (excitation: 485nm; emission: 530 nm). The expression
577 levels were calculated by dividing the intensity of fluorescence by the optical density at 600
578 nm, after subtracting the values of a blank sample. These results are given in arbitrary units
579 because the intensity of fluorescence is acquired with an automatic optimal gain and hence
580 varies from one experiment to the other.

581

582 **Lipid extraction and quinone analysis**

583 Cultures of 2, 5, or 10 mL were cooled on ice for at least 30 min before centrifugation
584 at 3200 x g at 4°C for 10 min. Cell pellets were washed in 1 mL ice-cold phosphate-buffer
585 saline (PBS) and transferred to preweighted 1.5 mL Eppendorf tubes. After centrifugation at
586 12,000 g at 4 °C for 1 min, the supernatant was discarded, the cell wet weight was
587 determined and pellets were stored at -20°C until lipid extraction, if necessary. Quinone
588 extraction from cell pellets was performed as previously described (6). The dried lipid
589 extracts were resuspended in 100 µL ethanol, and a volume corresponding to 1 mg of cell
590 wet weight was analyzed by HPLC electrochemical detection-MS (ECD-MS) with a BetaBasic-
591 18 column at a flow rate of 1 mL/min with a mobile phase composed of 50% methanol, 40%
592 ethanol, and 10% of a mix (90% isopropanol, 10% ammonium acetate (1 M), and 0.1% formic
593 acid). When necessary, MS detection was performed on an MSQ spectrometer (Thermo
594 Scientific) with electrospray ionization in positive mode (probe temperature, 400°C; cone
595 voltage, 80 V). Single-ion monitoring detected the following compounds: UQ₈ (M+H⁺), m/z
596 727-728, 6–10 min, scan time of 0.2 s; 3(¹⁸O)-UQ₈ (M+H⁺), m/z 733-734, 6–10 min, scan time
597 of 0.2 s; UQ₈ (M+NH₄⁺), m/z 744-745, 6–10 min, scan time of 0.2 s; UQ₁₀ (M+NH₄⁺), m/z 880–
598 881, 10-17 min. MS spectra were recorded between m/z 600 and 900 with a scan time of 0.3
599 s. ECD and MS peak areas were corrected for sample loss during extraction on the basis of

600 the recovery of the UQ₁₀ internal standard and then were normalized to cell wet weight. The
601 peaks of UQ₈ obtained with electrochemical detection or MS detection were quantified with
602 a standard curve of UQ₁₀ as previously described (6).

603

604 ¹⁸O₂ labeling

605 MG1655 wt and *ΔubiHΔubiF* containing respectively the pBAD24 empty vector or
606 pBAD-*ubiUV* were grown overnight at 37°C in LB medium supplemented with Ampicillin (100
607 μg/mL) and 0.05% arabinose. These precultures were used to inoculate 20 mL of the same
608 fresh medium at an optical density at 600 nm (OD₆₀₀) of 0.05 in Erlenmeyer flasks of 250 mL.
609 The cultures were grown at 37°C, 180 rpm, until an OD₆₀₀ of 0.4-0.5 was reached. An aliquot
610 was taken for lipid extraction and quinone analysis (0 min of ¹⁸O₂) and 13 mL of each culture
611 was transferred to an Hungate tube. 5 mL of labeled molecular oxygen (¹⁸O₂) was injected
612 through the septum with disposable syringes and needles, and the incubation was continued
613 at 37°C, 180 rpm for 2 hours. Then 5 mL of each sample was taken for quinone analysis (120
614 min of ¹⁸O₂).

615

616 Mouse intestine colonization experiments

617 All animal experiments were performed in accordance with the institutional and national
618 guidelines. Experiments were performed under the supervision of C.L. (agreement 38 10 38)
619 in the Plateforme de Haute Technologie Animale (PHTA) animal care facility (agreement
620 C3851610006 delivered by the Direction Départementale de la Protection des Populations)
621 and were approved by the ethics committee of the PHTA and by the French government
622 (APAFIS#14895- 2018042623275606.v5).

623 4-week-old female BALB/cByJ were purchased from Charles River Laboratories (Saint-
624 Germain-Nuelles) and were acclimatized in a controlled animal facility under specific
625 pathogen-free conditions for two weeks prior to the beginning of the colonization assay.
626 Mice were randomly assigned to groups of three or five per cage and ear punching was used
627 in order to identify each mouse in a given cage.

628 The colonization experiments were adapted and performed as previously described
629 (42, 43). Mice were given drinking water containing streptomycin sulfate and glucose (both 5
630 g/L) for 72 hours to remove existing resident anaerobic facultative microflora. For clearance

631 of streptomycin, fresh water devoid of antibiotic and glucose was then given to mice for 48
632 hours before inoculation of *E. coli* strains and for the rest of experiment. To start the
633 competition experiment, the mice were orally inoculated with 200 μ L of a mixture in a 1:1
634 ratio of the two competing strains at \sim 20,000 cells/mL in PBS. Mice from each cage were
635 orally inoculated with the same solution of bacteria. An aliquot of inoculum was plated on LB
636 agar containing 15 μ g/mL tetracycline in order to compute the input value.

637 The relative abundance of both competing strains was then monitored at several
638 days post-inoculation in fecal samples. Fecal samples were collected from each mouse in
639 preweighed 1.5 mL Eppendorf tubes containing the equivalent of 100 μ L glass beads
640 (diameter 0.25 to 0.5 mm) and 80 μ L PBS and the feces weight was determined. A volume of
641 PBS was then added to each tube in order to obtain a final concentration of 0.15 g of feces
642 per 1 mL PBS. The feces were homogenized by vortexing for 2 min, serially diluted by 10-fold
643 steps up to a 10^5 -fold dilution, and aliquots of 70 μ L were plated on LB agar medium
644 containing 15 μ g/mL tetracycline. The plates were incubated overnight at 37°C and were
645 transferred at 4°C for at least 2 hours the following day, before imaging under blue light
646 which revealed the fluorescent markers carried by each colony. The red and green colonies
647 corresponding respectively to MP7 and MP13 strains were counted by an adapted version of
648 ImageJ. Then, the CFU was computed per gram of feces for each strain and a competitive
649 index (CI) was calculated as a ratio of (MP13 mutant CFU/MP7 wt CFU) / (input MP13
650 mutant CFU/input MP7 wt CFU), where the input CFU was determined from the inoculum
651 for which an aliquot was plated on the day of gavage. The limit of detection in fecal plate
652 counts was 10^2 CFU/g feces. At all-time points, the wt strain was detectable on the fecal
653 plates. The absence of CFU count and CI for one day in one mouse corresponds to the
654 absence of feces for that day. Significance of CI was calculated by GraphPad Prism using one-
655 sample t test compared to one.

656 **Acknowledgements**

657 We thank Marc Fontecave and Murielle Lombard from College de France, and the members
658 of the SAME unit at Pasteur for discussion and help. We thank Mark Goulian (University of
659 Pennsylvania, USA) for providing the MP7 and MP13 *E. coli* strains and Laurent Loiseau for
660 providing the UbiUVT SPA-tagged strains. We gratefully acknowledge the help of TrEE team
661 members with the mouse intestine colonization experiments, Françoise Blanquet, Dalil
662 Hannani, Clément Caffaratti, and Amélie Amblard. We are also grateful to Arnold Fertin for
663 developing the ImageJ plugin used for the automatic counting of red and green colonies.
664 This project was supported by Institut Pasteur and CNRS and by grants from the ANR (ANR-
665 10-LABX-62-IBEID and ANR-19-CE44-0014O2-TABOO).
666

667 **Table 1: Strains used in this study**

668

Strain	Genotype	Construction	Reference
FBE051	MG1655		Lab strain
FBE229	<i>ΔubiUV::kan</i>	PCR LL792/LL715 on pKD4, recombined in BW25113, followed by Φ P1 transduction in MG1655	This work
FBE230	<i>ΔubiUV::cat</i>	PCR LL792/LL715 on pKD3, recombined in BW25113, followed by Φ P1 transduction in MG1655	This work
FBE254	<i>ΔubiT::kan</i>		(3)
FBE255	<i>ΔubiT::cat</i>		(3)
FBE354	<i>Δfnr::aadA</i>		(44)
FBE430	<i>ΔmenA::kan</i>	Φ P1 transduction from Keio <i>ΔmenA</i> to MG1655	This work
FBE501	<i>ΔmenA</i>	kanamycin cassette removed from FBE430 with pCP20	This work
FBE526	<i>ΔmenA ΔubiT::kan</i>	Φ P1 transduction from FBE254 to FBE501	This work
FBE527	<i>ΔmenA ΔubiUV::kan</i>	Φ P1 transduction from FBE229 to FBE501	This work
FBE947	<i>ΔubiH::Kan ΔubiUV::cat</i>	Φ P1 transduction from FBE230 to FBE253	This work
FBE1013	<i>ΔmenA ΔubiH::kan</i>	Φ P1 transduction from FBE253 to FBE501	This work
FBE1032	<i>ΔpyrD::kan</i>	Φ P1 transduction from Keio <i>ΔpyrD</i> to MG1655	This work
FBE253	<i>ΔubiH::kan</i>		(13)
FBE510	<i>ΔubiD::cat</i>		(3)
FBE512	<i>ΔubiF::kan</i>		(6)
FBE515	<i>ΔubiK::kan</i>		(45)
FBE518	<i>ΔubiA::cat</i>		(3)
FBE690	<i>Δubil</i>	Φ P1 transduction from Keio <i>Δubil</i> to MG1655 then kanamycin cassette removed with pCP20	This work
FBE713	<i>ΔubilK</i>	Φ P1 transduction from FBE515 to FBE690	This work
FBE576	<i>ΔubilFΔubiHF::cat</i>		(13)
FBE650	<i>ΔubilHF</i>	FBE576 strain cured with pCP20 plasmid	This work
FBE514	<i>ΔubiJ::cat</i>		(46)
FBE794	<i>ΔubiJΔubiH</i>	Φ P1 transduction from FBE514 to FBE253	This work
FBE264	<i>ΔubiJΔubiF</i>	Φ P1 transduction from FBE514 to FBE512	This work
FBE795	<i>ΔubiTΔubiH</i>	Φ P1 transduction from FBE255 to FBE253	This work
FBE265	<i>ΔubiTΔubiF</i>	Φ P1 transduction from FBE255 to FBE512	This work
FBE792	<i>ΔubiHΔubiA</i>	Φ P1 transduction from FBE518 to FBE253	This work
FBE793	<i>ΔubiHΔubiD</i>	Φ P1 transduction from FBE510 to FBE253	This work
FBE656	<i>ubiU-SPA-kan</i>	Φ P1 transduction DY330ubiU-SPA in MG1655	This work
FBE789	<i>ubiV-SPA-kan</i>	Φ P1 transduction DY330ubiV-SPA in MG1655	This work

FBE655	<i>ubiT</i> -SPA-kan	Recombination PCR LL711/LL712 on pJL148 in BW25113 then Φ P1 transduction in MG1655	This work
FBE695	Δ <i>fnr ubiU</i> -SPA-kan	Φ P1 transduction from FBE656 to FBE354	This work
FBE696	Δ <i>fnr ubiV</i> -SPA-kan	Φ P1 transduction from FBE789 to FBE354	This work
FBE694	Δ <i>fnr ubiT</i> -SPA-kan	Φ P1 transduction from FBE655 to FBE354	This work
FBE882	<i>ubiT</i> -SPA mutF1	Recombination pKO3- <i>ubiTU</i> mutF1 (pVP222) in FBE655	This work
FBE883	<i>ubiT</i> -SPA mut Δ F2	Recombination pKO3- <i>ubiTU</i> mut Δ F2 (pVP223) in FBE655	This work
FBE884	<i>ubiV</i> -SPA mutF1	Recombination pKO3- <i>ubiTU</i> mutF1 (pVP222) in FBE789	This work
FBE885	<i>ubiV</i> -SPA mut Δ F2	Recombination pKO3- <i>ubiTU</i> mut Δ F2 (pVP223) in FBE789	This work
FBE855	<i>yhbS</i> -SPA-kan	Recombination PCR <i>ebp292/293</i> on pJL148 in BW25113 then Φ P1 transduction in MG1655	This work
FBE856	Δ <i>fnr yhbS</i> -SPA-kan	Φ P1 transduction from FBE856 to FBE354	This work
FBE857	Δ <i>yhbS</i>	Φ P1 transduction from Keio Δ <i>yhbS</i> to MG1655	This work
FBE858	Δ <i>yhbS</i> Δ <i>menA</i>	Φ P1 transduction from Keio Δ <i>yhbS</i> to FBE354	This work
FBE484	MP7	Lambda att : tetR tetA-mCherry	(27)
FBE485	MP13	Lambda att : tetR tetA-gfpmut3.1	(27)
FBE550	<i>MP13</i> Δ <i>ubiUV</i>	Φ P1 transduction from FBE229 to FBE485	This work
FBE888	<i>MP13</i> Δ <i>menA</i>	Φ P1 transduction from FBE430 to FBE485	This work

669

670

671 **Table 2: Plasmids used in this study.**

672

Plasmid	Name	Description / Construction	Source
pCP20	pCP20	Ap, Cm, FLP recombinase expression	(39)
pEB227	pBAD24	AmpR – ColE1 ori – PBAD promoter	(41)
pEB267	pKD46	AmpR – ts ori – lambda Red genes	(38)
pEB268	pKD3	AmpR – FRT-cat-FRT	(38)
pEB269	pKD4	AmpR – FRT-kanaR-FRT	(38)
pEB794	pJL148	AmpR – SPA-FRT-kanaR-FRT	(18)
pES154	pBAD- <i>ubiUV</i>	PCR on MG1655 genomic DNA <i>ebp134/136</i> (EcoRI/XhoI) in pBAD24 (EcoRI/SalI)	This work
pES185	pBAD- <i>ubiU</i> (C176A) <i>V</i>	Mutagenesis PCR <i>ebp178/179</i> on pES154	This work
pES184	pBAD- <i>ubiUV</i> -SPA	PCR <i>ebp134/ebm968</i> on strain FBE696(EcoRI/XhoI) in pBAD24 (EcoRI/SalI)	This work
pVP040	pBAD- <i>fnr</i>	PCR on MG1655 genomic DNA <i>ebp31/32</i> (MfeI/XhoI) in pBAD24 (EcoRI/SalI)	This work
pEB1242	pASK-IBA37plus	AmpR – ColE1 ori – TetR promoter – 6His	IBA
pEB1823	pTet	PCR mutagenesis <i>ebm1567/1568</i> on pEB1242 to remove 6His tag	This work
pES060	pTet- <i>ubil</i>	PCR on MG1655 genomic DNA <i>ebp64/65</i> (EcoRI/XhoI) in pTet (EcoRI/XhoI)	This work
pES059	pTet- <i>ubiH</i>	PCR on MG1655 genomic DNA <i>ebp61/62</i> (EcoRI/XhoI) in pTet (EcoRI/XhoI)	This work
pES143	pTet- <i>ubiF</i>	PCR on MG1655 genomic DNA <i>ebp37/38</i> (EcoRI/XhoI) in pTet (EcoRI/XhoI)	This work
pES151	pTet- <i>ubiM</i> _Neisseria	PCR on MG1655 genomic DNA <i>ebp139/140</i> (EcoRI/XhoI) in pTet (EcoRI/XhoI)	This work
pEB898	pUA66	KanR - pSC101 ori - GFPmut2	(20)
	pUA- <i>ubiUVp</i>		(20)
pVP220	pUA- <i>ubiUVp</i> mutF1	Mutagenesis PCR <i>Ebp287/288</i> on pUA- <i>ubiU</i>	This work
	pUA- <i>ubiTp1p2</i>		(20)
pVP169	pUA- <i>ubiTp1</i>	PCR on MG1655 genomic DNA <i>ebp191/192</i> (XhoI/BamHI) in pUA66 (XhoI/BamHI)	This work
pVP170	pUA- <i>ubiTp2</i>	PCR on MG1655 genomic DNA <i>ebp193/194</i> (XhoI/BamHI) in pUA66 (XhoI/BamHI)	This work
pVP187	pUA- <i>ubiTp1p2</i> ΔF2	Mutagenesis PCR <i>Ebp237/238</i> on pUA- <i>ubiT</i>	This work
pVP221	pUA- <i>ubiTp1p2</i> mutF2	Mutagenesis PCR <i>Ebp289/290</i> on pUA- <i>ubiT</i>	This work
pEB232	pKO3	camR, pSC101 ori, <i>sacB</i>	(40)
pVP219	pKO3- <i>ubiTU</i>	PCR on MG1655 genomic DNA <i>ebp276/291</i> (XhoI/BamHI) in pKO3 (SalI/BamHI)	This work
pVP222	pKO3- <i>ubiTU</i> mutF1	Mutagenesis PCR <i>ebp287/288</i> on pVP219	This work
pVP223	pKO3- <i>ubiTU</i> mutΔF2	Mutagenesis PCR <i>ebp237/238</i> on pVP219	This work

673

674

675 **Table 3 : Primers used in this study.**

Primers	sequence	use
ebm968	ttgctcgagAAGCAGCTCCAGCCTACACG	<i>ubiV</i> -SPA RV
ebm1567	GAAATAATTTTGTAACTTTAAGAAGGAGATGAATTCGAGCTCGGTACCCG	pEB1823
ebm1568	CGGGTACCGAGCTCGAATTCATCTCCTTCTTAAAGTTAAACAAAATTATTC	pEB1823
Ebp31	GAGCAATTGatgATCCCGAAAAGCGAATTATAC	<i>fnr</i> FW MfeI
Ebp32	acgctcgagtcaGGCAACGTTACGCGTATG	<i>fnr</i> RV XhoI
Ebp37	actgaattcatgACAAATCAACCAACGGAAATTG	<i>ubiF</i> FW EcoRI
Ebp38	acgctcgagctaCAACCCTAACGCATATTTTCAGC	<i>ubiF</i> RV XhoI
Ebp61	actgaattcATGAGCGTAATCATCGTCGGTG	<i>ubiH</i> FW EcoRI
Ebp62	acgctcgagTtAACGCGCCACCCAACC	<i>ubiH</i> RV XhoI
Ebp64	actgaattcATGCAAAGTGTGATGTAGCCATTG	<i>ubil</i> FW EcoRI
Ebp65	acgctcgagTTAACGCAGCCATTCAGGCAAATC	<i>ubil</i> RV XhoI
Ebp134	actgaattcatgGAGCTGCTCTGCCCTG	<i>ubiU</i> FW EcoRI
Ebp136	actgaattcATGAAATATTCCTTAGGGCCAGTG	<i>ubiV</i> RV XhoI
Ebp139	actgaattcATGGGTTTTGATATAATCGCCTATC	<i>ubiM</i> FW EcoRI
Ebp140	acgctcgagTCAACCGGTCAGTTGTTGGTAATC	<i>ubiM</i> RV XhoI
Ebp178	TTATGTCCGAAGGTCGTgCTATCTGTCTGTCGTATC	<i>ubiU</i> (C179A) FW
Ebp179	GATACGACGACAGATAGgcACGACCTTCGACATAA	<i>ubiU</i> (C179A) RV
Ebp191	acgctcgagTTAAGCGCCGGGAGATTTCC	<i>ubiTp1</i> FW
Ebp192	cgggatccTGCTGCTACCACCAATACAAC	<i>ubiTp1</i> RV
Ebp193	cgggatccTTTTAGCGCAAATGGCGTCAG	<i>ubiTp2</i> RV
Ebp194	acgctcgagAGCAGCAATTTTCATATGGAATTGTTG	<i>ubiTp2</i> FW
Ebp237	ttggtgtagcagcaatttcatatggaattgctatgttatttttctgat	mutΔ <i>Fnr</i> 2 FW
Ebp238	atcagaaaaataacatagcaatttcatatgaaattgctgctaccaccaa	mutΔ <i>Fnr</i> 2 RV
Ebp275	actgaattcaTGTTGGATAAACTGCGTTC	<i>ubiT</i> FW
Ebp276	acgctcgagTTAGCATGGTTCACCTACCGATG	<i>ubiT</i> RV XhoI
Ebp285	acgctcgagTTAAAAGCGATTGAAATGCTCG	<i>yhbS</i> RV
Ebp287	CAACTTAACTGCCTTAAtcatcAAATTGTCGCAGCAAG	mut <i>Fnr</i> 1 FW
Ebp288	CTTGCTGCGACAATTTgatgaTTAAGGCAGTTAAAGTTG	mut <i>Fnr</i> 1 RV
Ebp289	CAGCAATTTTCATATGGAATTGcatgaTTATACCGCTATGTTATTTTTC	mut <i>Fnr</i> 2 FW
Ebp290	GAAAAATAACATAGCGGTATAAtcatgCAATTCATATGAAATTGCTG	mut <i>Fnr</i> 2 RV
Ebp291	cgggatccTACGACGACAGATAGCAACGAC	<i>ubiU</i> RV BamHI
Ebp292	GGCGTTACCGGCCTGGTTGAGTATCACGAGCATTTCATCGCTTTTCCATGGA AAAGAGAAG	<i>yhbS</i> -tag FW
Ebp293	GCGCAGGGTTTGCAGAGCTGTTAAGCAGTCTGCAAACCCCGGAGACATATG AATATCCTCCTTAG	<i>yhbS</i> -tagRV
LL710	AAAACCGCGCTGAAACCAACAGACATCGGTAGGTGAACCATGCTCCATGG	<i>ubiT</i> -tag FW
LL711	GCAGGGCATCAATACCCGGCGCATCAATGGGAATTTCTACTCGAACATATGA ATATCCTCCTTAG	<i>ubiT</i> -tagRV
LL715	aaagagtagttaaagttgtaacaaagtgagctatttacCATATGAATATCCTCCTTA	RV <i>ubiV</i> Wanner
LL792	catttttgcgttttgatagcgcaaccttcaggaataattGTGTAGGCTGGAGCTGCTTC	FW <i>ubiU</i> Wanner

676

677 **LEGENDS**

678

679 **Figure 1. Complementation of *ubiI*, *ubiH*, and *ubiF* mutants by pBAD-*ubiUV* in the presence**
680 **of O₂. (A).** *E. coli* mutant strains $\Delta ubiH$ (FBE253), $\Delta ubiF$ (FBE512), $\Delta ubiIK$ (FBE713), and
681 $\Delta ubiIH\Delta ubiF$ (FBE650) were transformed by pBAD24 (e.v.), pBAD-UbiUV, and pBAD-
682 UbiU(C176A)V plasmids. **(B).** *E. coli* mutant strains $\Delta ubiH\Delta ubiA$ (FBE792), $\Delta ubiH\Delta ubiD$
683 (FBE793), and $\Delta ubiH$ (FBE253) were transformed by pBAD24 (e.v.) and pBAD-UbiUV. (A-B)
684 After selection in the absence of O₂, cultures were washed and serially diluted in minimal
685 medium then spotted on M9 succinate plates containing 0.02% arabinose, and incubated at
686 37°C for 48 hours (or 96 hours for the $\Delta ubiIHF$ series) in aerobic conditions (21% O₂). The
687 results shown are representative of at least two independent experiments.

688

689 **Figure 2. Complementation of *ubiH* and *ubiF* mutants by pBAD-UbiUV is *ubiT* dependent**
690 **(and *ubiJ* independent).** *E. coli* mutant strains were transformed by pBAD24 (e.v.) and pBAD-
691 UbiUV plasmids. After selection in the absence of O₂, cultures were washed and serially
692 diluted in minimal medium then spotted on M9 succinate plates containing 0.02% arabinose
693 at 37°C in aerobic conditions. The results shown are representative of at least two
694 independent experiments. **(A)** strains $\Delta ubiJ$ (FBE514) and wt **(B)** strains $\Delta ubiH$ (FBE253),
695 $\Delta ubiH\Delta ubiJ$ (FBE794), and $\Delta ubiH\Delta ubiT$ (FBE795); **(C)** strains $\Delta ubiF$ (FBE512), $\Delta ubiF\Delta ubiJ$
696 (FBE264), $\Delta ubiF\Delta ubiT$ (FBE265), and wt.

697

698 **Figure 3. UbiUV restore the UQ₈ content of $\Delta ubiIH$ and $\Delta ubiF$ mutants without using O₂ for**
699 **the hydroxylation steps. (A)** UQ₈ content of the indicated strains containing either pBAD
700 (e.v.), pBAD-*ubiUV*, or pBAD-*ubiU(C176A)V* after aerobic growth overnight at 37°C in LB
701 medium. *E. coli* wt strain (MG1655) containing the empty vector was used as control. Mean
702 \pm standard deviations (SD) (n=3 to 4). ***, P < 0.001; ****, P < 0.0001 by unpaired Student's
703 t test. **(B-F)** Detection of UQ₈ with ¹⁸O₂ labelling. **(B)** Quantification of UQ₈ content in wt
704 (MG1655) cells containing an empty vector (e.v.) and in $\Delta ubiIH\Delta ubiF$ cells containing the
705 pBAD-*ubiUV* vector just before (0 min) and two hours (120 min) after adding ¹⁸O₂. Mean \pm
706 SD (n=2). **(C to F)** Mass spectra of UQ₈ from cells shown in B, wt **(C and E)** and $\Delta ubiIH\Delta ubiF$
707 with pBAD-*ubiUV* **(D and F)**, before **(E and F)** and two hours after **(E and F)** addition of ¹⁸O₂.
708 Mass spectra representative of two independent experiments.

709 **Figure 4. Fnr controls UbiTUV expression and UQ biosynthesis under anaerobiosis. (A,B).** *E.*
710 *coli* strains UbiU-SPA, UbiV-SPA, and UbiT-SPA, and their corresponding Δfnr versions (strains
711 FBE656, FBE789, FBE655, FBE695, FBE696, FBE694) were grown in LB at 37°C in +O₂ and -O₂
712 (A) or in +O₂ and 0.1% O₂ (B) and analyzed by Western blot: normalized quantities of total
713 protein extracts (in biological duplicate) were separated by SDS-PAGE 12% and detected by
714 Western-Blot using anti-Flag monoclonal antibody for the detection of the SPA tag (green) or
715 anti-YbgF polyclonal antibodies as an internal loading control (red). (C). UQ₈ content of the
716 wild type and Δfnr (FBE354) strains was assayed after aerobic or anaerobic growth overnight
717 at 37°C in LB medium. Mean \pm standard deviations (SD) (n=3 to 4). ****, P < 0.0001 by
718 unpaired Student's t test.

719

720 **Figure 5. (A). Organization of the promoter region of *ubiTUV* genes.** The sequence of the
721 intergenic region between *ubiU* and *ubiT* genes is shown, from the start codon of *ubiU*, to
722 the start codon of *ubiT* (both indicated in bold at the extremities of the sequence). The
723 transcription start sites as determined in (19), are indicated in red. The two Fnr binding sites
724 F1 and F2 are indicated in green. The mutF1, mutF2, and mut Δ F2 mutations introduced in
725 the transcriptional fusions are depicted in red. (B). **Limits of transcriptional fusions used in**
726 **panels C-E. (C-E). Activity of the transcriptional fusions with or without *fnr* expression.** Δfnr
727 *E. coli* strain was co-transformed by pBAD24 or pBAD-*fnr* together with the indicated
728 transcriptional fusions. After overnight growth of 4 biological replicates at 37°C in LB in
729 anaerobiosis, GFP levels were quantified. Errors bars indicate the standard deviation. *, P <
730 0.1; **, P < 0.01; ****, P < 0.0001 by unpaired Student's t test. (F). **Role of the Fnr sites in**
731 **UbiTUV physiological levels.** *E. coli* strains UbiV-SPA and UbiT-SPA, without (wt) or with the
732 indicated mutation in the F1 or F2 binding sites, were grown in LB overnight at 37°C in the
733 absence of O₂. Normalized quantities of total protein extracts (in biological triplicate) were
734 separated by 12% SDS-PAGE and detected by Western-Blot using anti-Flag monoclonal
735 antibody for the detection of the SPA tag (green) or anti-YbgF polyclonal antibody as an
736 internal loading control (red).

737

738 **Figure 6. Role of *ubiUVT* in anaerobic growth.** *E. coli* wt and strains devoid of the MK/DMK
739 ($\Delta menA$), UQ synthesis pathways – aerobic ($\Delta ubiH$) and anaerobic ($\Delta ubiUV$ or $\Delta ubiT$) – and
740 controls for anaerobic growth (Δfnr) and auxotrophy for uracil ($\Delta pyrD$) were grown

741 aerobically at 37°C in LB medium or LB glucose 0.2% (for $\Delta menA \Delta ubiH$), washed and
742 resuspended in M9 medium without carbon source to OD₆₀₀ 1. Serial dilutions were spotted
743 in agarose M9 medium plates supplemented with carbon source (glycerol or glucose), KNO₃
744 or Uracil and incubated at 37°C at the indicated O₂ concentration until growth was observed.
745 Experiments were performed in triplicates and confirmed with at least 4 independent
746 biological replicates.

747

748 **Figure 7. Quinones contribute differently to colonization of the mouse gut by *E. coli*. (A).**

749 Schematic representation of the experimental protocol for the mouse intestine colonization
750 competitions, adapted from (42). (B-C) Total CFU counts (B) and associated competitive
751 index (C) in feces of mice after oral co-inoculation with a 1:1 ratio of MP7 wt and MP13
752 $\Delta ubiUV$ strains. (D-E) same as B-C with MP7 wt and MP13 $\Delta menA$ strains. The limit of
753 detection of 10² CFU is indicated as dotted line. Mean \pm standard deviations (SD), each white
754 circle represents values for individual mice (n=5 and 8), circles missing corresponds to the
755 absence of feces for that day. ns, not significant; *, P < 0.05; **, P < 0.01; ***, P < 0.001;
756 ****, P < 0.0001 by one-sample t test. Changes in total CFU counts and CI throughout the
757 experiment in each mouse are shown in Figure S6.

758

759 **Figure 8. Role of *ubiUVT* in the anaerobic to aerobic transition. (A).** *E. coli* wt and strains

760 devoid of the MK/DMK ($\Delta menA$) and UQ aerobic ($\Delta ubiH$) and anaerobic ($\Delta ubiUV$ or $\Delta ubiT$)
761 synthesis pathways, were grown anaerobically in LB KNO₃ medium, washed in M9 medium
762 without carbon source and resuspended in M9 succinate medium to OD₆₀₀=0.02. Growth
763 was followed aerobically at 37°C in a TECAN microplate reader in 3 independent
764 experiments. At 40 hours of growth, cells were diluted 1/100 in the same medium (refresh)
765 and growth was resumed for 20h more. (B). *E. coli* wt (MG1655), $\Delta ubiUV$ and $\Delta ubiT$ strains
766 were cultured anaerobically in LB medium containing NO₃⁻ as final electron acceptor until OD
767 ~ 1. After 20 min of treatment with chloramphenicol (+Clp) at 200 μ g/mL or without
768 chloramphenicol (-Clp) under anaerobic conditions, the cultures were shifted to ambient air
769 for a two-hour incubation. UQ₈ content was quantified before (0 min) or after oxic transition
770 (30 min and 120 min) by HPLC-ECD of lipid extracts from 1 mg of cells. Quantifications are
771 expressed as picomole per milligram of cells (n=4 biological replicates). **, P < 0.01; ***, P <
772 0.001 by unpaired Student's t test. Mean \pm standard deviation is indicated.

773

774 **Figure S1. O₂-dependent and O₂-independent biosynthetic pathways of UQ in *E. coli*.** R,
775 octaprenyl chain illustrated on the UQ₈ structure; 4-HB, 4-hydroxybenzoic acid; OPP, 3-
776 octaprenylphenol; DMQ₈, C-6-demethoxyubiquinone; DMAPP, dimethylallyl pyrophosphate;
777 IPP, isopentenyl pyrophosphate. The Ubi-enzymes and accessory factors common between
778 the two pathways are in black, those corresponding to the aerobic pathway in red, and those
779 corresponding to the anaerobic pathway are in blue. Hydroxyl groups added on C5, C1, and
780 C6 are highlighted in red.

781

782 **Figure S2. Amount of UbiV-SPA produced in +O₂ from pBAD-UbiUV-SPA plasmid compared**
783 **with physiological amount in -O₂ of chromosome-encoded UbiV-SPA.** Strain UbiV-SPA
784 (FBE789) was grown in LB in the absence of O₂. Wild type *E. coli* transformed by pBAD-
785 UbiUV-SPA (pES184) was grown in LB in +O₂ and induced 2 hours with 0.02% arabinose.
786 After preparation of whole cell extract, the sample was diluted 2-fold serially (1 to 1/32).
787 Western blot was performed using an anti-Flag antibody. ni : uninduced cells.

788

789 **Figure S3.** Ubiquinone 8 (UQ₈), demethylmenaquinone 8 (DMK₈) and menaquinone 8 (MK₈)
790 content in the indicated mutant strains of the Keio collection (37) after anaerobic growth
791 overnight at 37°C in LB medium. Mean ± standard deviations (SD) (n=2).

792

793 **Figure S4. Comparison of UbiT-SPA levels in the regulation mutants in -O₂ and in +O₂.** *E.*
794 *coli* strains expressing UbiT-SPA with or without the Δfnr or $\text{mut}\Delta F2$ chromosomal mutations
795 (FBE655, FBE694, and FBE883) were grown in biological duplicates in LB at 37°C in the
796 indicated oxygenic conditions until OD_{600nm}=1. Normalized quantities of total protein
797 extracts in duplicate were separated by SDS-PAGE 12% and detected by Western-Blot using
798 anti-Flag monoclonal antibody for the detection of the SPA tag or anti-YbgF polyclonal
799 antibodies as an internal loading control.

800

801 **Figure S5. (A)** Ubiquinone 8 (UQ₈), **(B)** demethylmenaquinone 8 (DMK₈) and **(C)**
802 menaquinone 8 (MK₈) content in MP7 wt, MP13 $\Delta ubiUV$, MP13 $\Delta menA$ strains after
803 anaerobic **(A)** and aerobic **(B and C)** growth overnight at 37°C in LB medium. Mean ±
804 standard deviations (SD) (n=2). N.D., not detected.

805

806 **Figure S6.** Total CFU count per gram of feces (**A and B**) and competitive index (**C and D**) for
807 either MP7 (mCherry-tagged MP1) WT:MP13 (GFP-tagged MP1) $\Delta ubiUV$ (**A and C**) or MP7
808 WT:MP13 $\Delta menA$ (**B and D**) competition experiments in each mouse of the experiments
809 shown in Figure 7. The limit of detection was 10^2 CFU. The absence of total CFU count in one
810 day corresponds to the absence of feces for that day.

811

812 **Figure S7. Protein levels of UbiHF proteins in aerobic and anaerobic conditions.** Strains
813 producing UbiI, UbiH, and UbiF tagged with SPA at the chromosome, were grown in LB in
814 aerobic and anaerobic conditions. Whole cell extracts were analyzed by Western blot with
815 an anti-Flag antibody. Results representative of two independent experiments.

816

817 **Figure S8. *ubiT* is in operon with the unknown function *yhbS* gene. (A).** Genetic
818 organization. See legend of figure 5. **(B).** RT-PCRs were performed on total RNA prepared on
819 MG1655 cells in exponential phase, with oligonucleotides ebp275 and ebp285 (Table 3). The
820 positions of hybridization of the oligonucleotides are indicated in panel A. +/- RT indicates
821 the absence or presence of the reverse transcriptase (RT) enzyme in the reaction mixture. A
822 control PCR was performed on genomic DNA with the same oligonucleotides. **(C).** *E. coli*
823 strains YhbS-SPA and Δfnr /YhbS-SPA (FBE855, FBE856) were grown in LB at 37°C in the
824 indicated oxygenic conditions until $OD_{600nm}=1$. Normalized quantities of total protein
825 extracts in duplicate were separated by SDS-PAGE 12% and detected by Western-Blot using
826 anti-Flag monoclonal antibody for the detection of the SPA tag. **D.** The indicated *E. coli*
827 strains were grown anaerobically for two days at 37°C on M9 medium plates supplemented
828 with 0.2% glycerol and NO_3^- .

829

830 REFERENCES

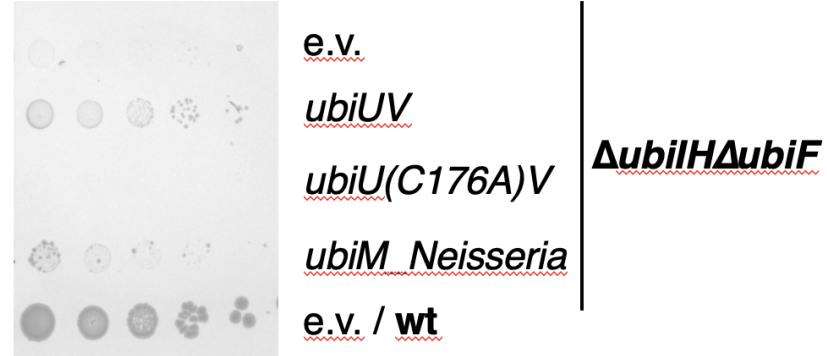
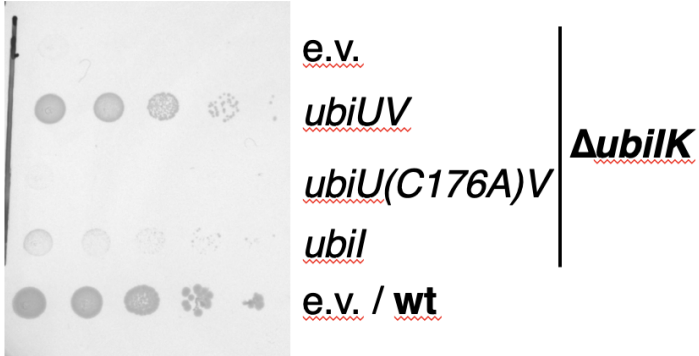
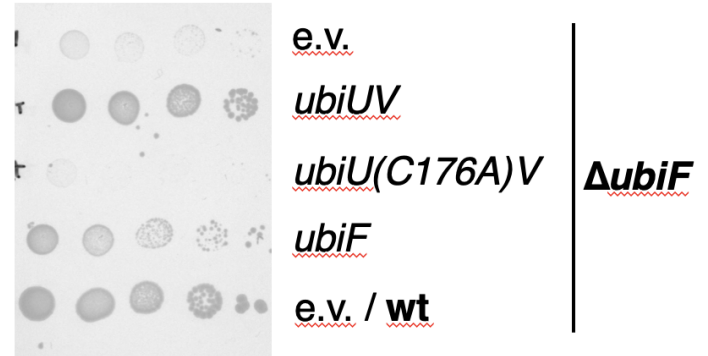
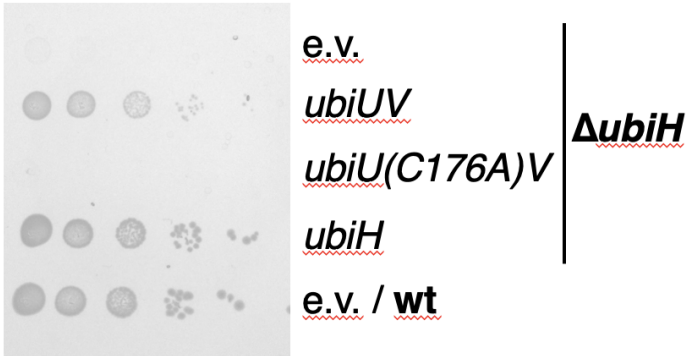
831

- 832 1. Kawamukai, M. 2018. Biosynthesis and applications of prenylquinones. *Biosci*
833 *Biotechnol Biochem* 82:963–977.
- 834 2. Franza, T, Gaudu, P. 2022. Quinones: more than electron shuttles. *Res Microbiol*
835 173:103953.
- 836 3. Pelosi, L, Vo, CD, Abby, SS, Loiseau, L, Rascalou, B, Hajj Chehade, M, Faivre, B,
837 Goussé, M, Chenal, C, Touati, N, Binet, L, Cornu, D, Fyfe, CD, Fontecave, M, Barras,
838 F, Lombard, M, Pierrel, F. 2019. Ubiquinone Biosynthesis over the Entire O₂ Range:
839 Characterization of a Conserved O₂-Independent Pathway. *mBio* 10
- 840 4. Abby, SS, Kazemzadeh, K, Vragliau, C, Pelosi, L, Pierrel, F. 2020. Advances in
841 bacterial pathways for the biosynthesis of ubiquinone. *Biochim Biophys Acta Bioenerg*
842 1861:148259.
- 843 5. Alexander, K, Young, IG. 1978. Three hydroxylations incorporating molecular oxygen
844 in the aerobic biosynthesis of ubiquinone in *Escherichia coli*. *Biochemistry* 17:4745–
845 4750.
- 846 6. Hajj Chehade, M, Loiseau, L, Lombard, M, Pecqueur, L, Ismail, A, Smadja, M,
847 Golinelli-Pimpaneau, B, Mellot-Draznieks, C, Hamelin, O, Aussel, L, Kieffer-Jaquinod,
848 S, Labessan, N, Barras, F, Fontecave, M, Pierrel, F. 2013. *ubiI*, a new gene in
849 *Escherichia coli* coenzyme Q biosynthesis, is involved in aerobic C5-hydroxylation. *J*
850 *Biol Chem* 288:20085–20092.
- 851 7. Kwon, O, Kotsakis, A, Meganathan, R. 2000. Ubiquinone (coenzyme Q) biosynthesis in
852 *Escherichia coli*: identification of the *ubiF* gene. *FEMS Microbiol Lett* 186:157–161.
- 853 8. Asquith, CRM, Murray, NH, Pagliarini, DJ. 2019. ADCK3/COQ8A: the choice target of
854 the UbiB protein kinase-like family. *Nat Rev Drug Discov* 18:815.
- 855 9. Hajj Chehade, M, Pelosi, L, Fyfe, CD, Loiseau, L, Rascalou, B, Brugière, S,
856 Kazemzadeh, K, Vo, CD, Ciccone, L, Aussel, L, Couté, Y, Fontecave, M, Barras, F,
857 Lombard, M, Pierrel, F. 2019. A Soluble Metabolon Synthesizes the Isoprenoid Lipid
858 Ubiquinone. *Cell Chem Biol* 26:482–492.e7.
- 859 10. Sakai, Y, Kimura, S, Suzuki, T. 2019. Dual pathways of tRNA hydroxylation ensure
860 efficient translation by expanding decoding capability. *Nat Commun* 10:2858.
- 861 11. Kimura, S, Sakai, Y, Ishiguro, K, Suzuki, T. 2017. Biogenesis and iron-dependency of
862 ribosomal RNA hydroxylation. *Nucleic Acids Res* 45:12974–12986.
- 863 12. Lauhon, CT. 2019. Identification and Characterization of Genes Required for 5-
864 Hydroxyuridine Synthesis in *Bacillus subtilis* and *Escherichia coli* tRNA. *J Bacteriol*
865 201:e00433–19.
- 866 13. Pelosi, L, Ducluzeau, AL, Loiseau, L, Barras, F, Schneider, D, Junier, I, Pierrel, F.
867 2016. Evolution of Ubiquinone Biosynthesis: Multiple Proteobacterial Enzymes with
868 Various Regioselectivities To Catalyze Three Contiguous Aromatic Hydroxylation
869 Reactions. *mSystems* 1:e00091–16.
- 870 14. Agrawal, S, Jaswal, K, Shiver, AL, Balecha, H, Patra, T, Chaba, R. 2017. A genome-
871 wide screen in *Escherichia coli* reveals that ubiquinone is a key antioxidant for
872 metabolism of long-chain fatty acids. *J Biol Chem* 292:20086–20099.
- 873 15. Esquilin-Lebron, K, Dubrac, S, Barras, F, Boyd, JM. 2021. Bacterial Approaches for
874 Assembling Iron-Sulfur Proteins. *mBio* 12:e0242521.
- 875 16. Myers, KS, Yan, H, Ong, IM, Chung, D, Liang, K, Tran, F, Keleş, S, Landick, R, Kiley,
876 PJ. 2013. Genome-scale analysis of *Escherichia coli* FNR reveals complex features of
877 transcription factor binding. *PLoS Genet* 9:e1003565.

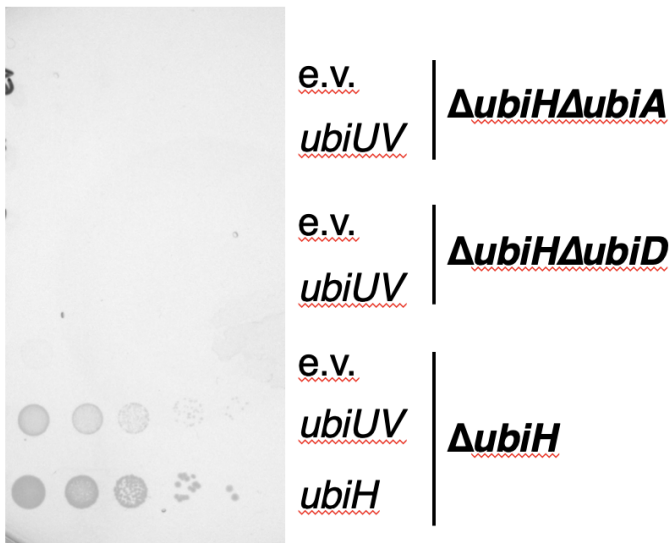
- 878 17. Federowicz, S, Kim, D, Ebrahim, A, Lerman, J, Nagarajan, H, Cho, BK, Zengler, K,
879 Palsson, B. 2014. Determining the control circuitry of redox metabolism at the genome-
880 scale. *PLoS Genet* 10:e1004264.
- 881 18. Zeghouf, M, Li, J, Butland, G, Borkowska, A, Canadien, V, Richards, D, Beattie, B,
882 Emili, A, Greenblatt, JF. 2004. Sequential Peptide Affinity (SPA) system for the
883 identification of mammalian and bacterial protein complexes. *J Proteome Res* 3:463–
884 468.
- 885 19. Thomason, MK, Bischler, T, Eisenbart, SK, Förstner, KU, Zhang, A, Herbig, A, Nieselt,
886 K, Sharma, CM, Storz, G. 2015. Global transcriptional start site mapping using
887 differential RNA sequencing reveals novel antisense RNAs in *Escherichia coli*. *J*
888 *Bacteriol* 197:18–28.
- 889 20. Zaslaver, A, Bren, A, Ronen, M, Itzkovitz, S, Kikoin, I, Shavit, S, Liebermeister, W,
890 Surette, MG, Alon, U. 2006. A comprehensive library of fluorescent transcriptional
891 reporters for *Escherichia coli*. *Nat Methods* 3:623–628.
- 892 21. Nitzschke, A, Bettenbrock, K. 2018. All three quinone species play distinct roles in
893 ensuring optimal growth under aerobic and fermentative conditions in *E. coli* K12.
894 *PLoS One* 13:e0194699.
- 895 22. Tseng, CP, Albrecht, J, Gunsalus, RP. 1996. Effect of microaerophilic cell growth
896 conditions on expression of the aerobic (*cyoABCDE* and *cydAB*) and anaerobic
897 (*narGHJI*, *frdABCD*, and *dmsABC*) respiratory pathway genes in *Escherichia coli*. *J*
898 *Bacteriol* 178:1094–1098.
- 899 23. Lambden, PR, Guest, JR. 1976. Mutants of *Escherichia coli* K12 unable to use fumarate
900 as an anaerobic electron acceptor. *J Gen Microbiol* 97:145–160.
- 901 24. Wallace, BJ, Young, IG. 1977. Role of quinones in electron transport to oxygen and
902 nitrate in *Escherichia coli*. Studies with a *ubiA*- *menA*- double quinone mutant.
903 *Biochim Biophys Acta* 461:84–100.
- 904 25. Sharma, P, Teixeira de Mattos, MJ, Hellingwerf, KJ, Bekker, M. 2012. On the function
905 of the various quinone species in *Escherichia coli*. *FEBS J* 279:3364–3373.
- 906 26. Newton, NA, Cox, GB, Gibson, F. 1971. The function of menaquinone (vitamin K 2) in
907 *Escherichia coli* K-12. *Biochim Biophys Acta* 244:155–166.
- 908 27. Lasaro, M, Liu, Z, Bishar, R, Kelly, K, Chattopadhyay, S, Paul, S, Sokurenko, E, Zhu, J,
909 Goulian, M. 2014. *Escherichia coli* isolate for studying colonization of the mouse
910 intestine and its application to two-component signaling knockouts. *J Bacteriol*
911 196:1723–1732.
- 912 28. Jones, SA, Gibson, T, Maltby, RC, Chowdhury, FZ, Stewart, V, Cohen, PS, Conway, T.
913 2011. Anaerobic respiration of *Escherichia coli* in the mouse intestine. *Infect Immun*
914 79:4218–4226.
- 915 29. Chen, J, To, L, de Mets, F, Luo, X, Majdalani, N, Tai, CH, Gottesman, S. 2021. A
916 fluorescence-based genetic screen reveals diverse mechanisms silencing small RNA
917 signaling in *E. coli*. *Proc Natl Acad Sci U S A* 118
- 918 30. Lee, JY, Tsolis, RM, Bäumlner, AJ. 2022. The microbiome and gut homeostasis. *Science*
919 377:eabp9960.
- 920 31. Knoell, HE. 1981. Stand-by position of the dioxygen-dependent ubiquinone-8 synthesis
921 apparatus in anaerobically grown *Escherichia coli* K-12. *FEMS Microbiology Letters*
922 10:59–62.
- 923 32. Vo, CD, Michaud, J, Elsen, S, Faivre, B, Bouveret, E, Barras, F, Fontecave, M, Pierrel,
924 F, Lombard, M, Pelosi, L. 2020. The O₂-independent pathway of ubiquinone
925 biosynthesis is essential for denitrification in *Pseudomonas aeruginosa*. *J Biol Chem*
926 295:9021–9032.

- 927 33. Cecchini, G, Schröder, I, Gunsalus, RP, Maklashina, E. 2002. Succinate dehydrogenase
928 and fumarate reductase from *Escherichia coli*. *Biochim Biophys Acta* 1553:140–157.
- 929 34. Möbius, K, Arias-Cartin, R, Breckau, D, Hännig, AL, Riedmann, K, Biedendieck, R,
930 Schröder, S, Becher, D, Magalon, A, Moser, J, Jahn, M, Jahn, D. 2010. Heme
931 biosynthesis is coupled to electron transport chains for energy generation. *Proc Natl*
932 *Acad Sci U S A* 107:10436–10441.
- 933 35. Jones, SA, Chowdhury, FZ, Fabich, AJ, Anderson, A, Schreiner, DM, House, AL,
934 Autieri, SM, Leatham, MP, Lins, JJ, Jorgensen, M, Cohen, PS, Conway, T. 2007.
935 Respiration of *Escherichia coli* in the mouse intestine. *Infect Immun* 75:4891–4899.
- 936 36. Hughes, ER, Winter, MG, Duerkop, BA, Spiga, L, Furtado de Carvalho, T, Zhu, W,
937 Gillis, CC, Büttner, L, Smoot, MP, Behrendt, CL, Cherry, S, Santos, RL, Hooper, LV,
938 Winter, SE. 2017. Microbial Respiration and Formate Oxidation as Metabolic
939 Signatures of Inflammation-Associated Dysbiosis. *Cell Host Microbe* 21:208–219.
- 940 37. Baba, T, Ara, T, Hasegawa, M, Takai, Y, Okumura, Y, Baba, M, Datsenko, KA,
941 Tomita, M, Wanner, BL, Mori, H. 2006. Construction of *Escherichia coli* K-12 in-
942 frame, single-gene knockout mutants: the Keio collection. *Mol Syst Biol* 2:2006.0008.
- 943 38. Datsenko, KA, Wanner, BL. 2000. One-step inactivation of chromosomal genes in
944 *Escherichia coli* K-12 using PCR products. *Proc Natl Acad Sci U S A* 97:6640–6645.
- 945 39. Cherepanov, PP, Wackernagel, W. 1995. Gene disruption in *Escherichia coli*: TcR and
946 KmR cassettes with the option of Flp-catalyzed excision of the antibiotic-resistance
947 determinant. *Gene* 158:9–14.
- 948 40. Link, AJ, Phillips, D, Church, GM. 1997. Methods for generating precise deletions and
949 insertions in the genome of wild-type *Escherichia coli*: application to open reading
950 frame characterization. *J Bacteriol* 179:6228–6237.
- 951 41. Guzman, LM, Belin, D, Carson, MJ, Beckwith, J. 1995. Tight regulation, modulation,
952 and high-level expression by vectors containing the arabinose PBAD promoter. *J*
953 *Bacteriol* 177:4121–4130.
- 954 42. Samuels, AN, Roggiani, M, Zhu, J, Goulian, M, Kohli, RM. 2019. The SOS Response
955 Mediates Sustained Colonization of the Mammalian Gut. *Infect Immun* 87:e00711–18.
- 956 43. Samuels, AN, Roggiani, M, Smith, KA, Zhu, J, Goulian, M, Kohli, RM. 2020.
957 Deciphering the Role of Colicins during Colonization of the Mammalian Gut by
958 Commensal *E. coli*. *Microorganisms* 8:E664.
- 959 44. Mettert, EL, Kiley, PJ. 2007. Contributions of [4Fe-4S]-FNR and integration host factor
960 to *fnr* transcriptional regulation. *J Bacteriol* 189:3036–3043.
- 961 45. Loiseau, L, Fyfe, C, Aussel, L, Hajj Chehade, M, Hernández, SB, Faivre, B, Hamdane,
962 D, Mellot-Draznieks, C, Rascalou, B, Pelosi, L, Velours, C, Cornu, D, Lombard, M,
963 Casadesús, J, Pierrel, F, Fontecave, M, Barras, F. 2017. The UbiK protein is an
964 accessory factor necessary for bacterial ubiquinone (UQ) biosynthesis and forms a
965 complex with the UQ biogenesis factor UbiJ. *J Biol Chem* 292:11937–11950.
- 966 46. Aussel, L, Loiseau, L, Hajj Chehade, M, Pocachard, B, Fontecave, M, Pierrel, F, Barras,
967 F. 2014. *ubiJ*, a new gene required for aerobic growth and proliferation in macrophage,
968 is involved in coenzyme Q biosynthesis in *Escherichia coli* and *Salmonella enterica*
969 serovar Typhimurium. *J Bacteriol* 196:70–79.
- 970

A



B



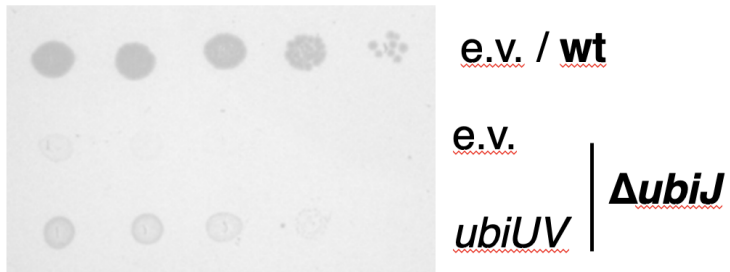
e.v.
ubiUV

$\Delta ubiH\Delta ubiD$

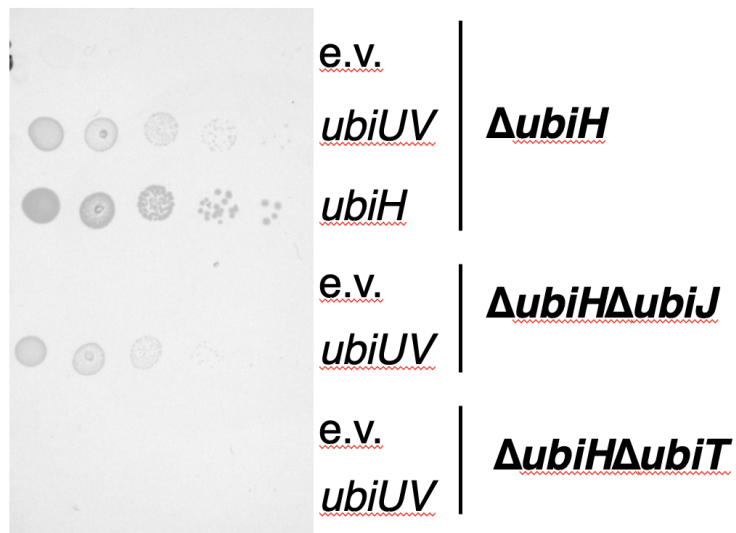
e.v.
ubiUV
ubiH

$\Delta ubiH$

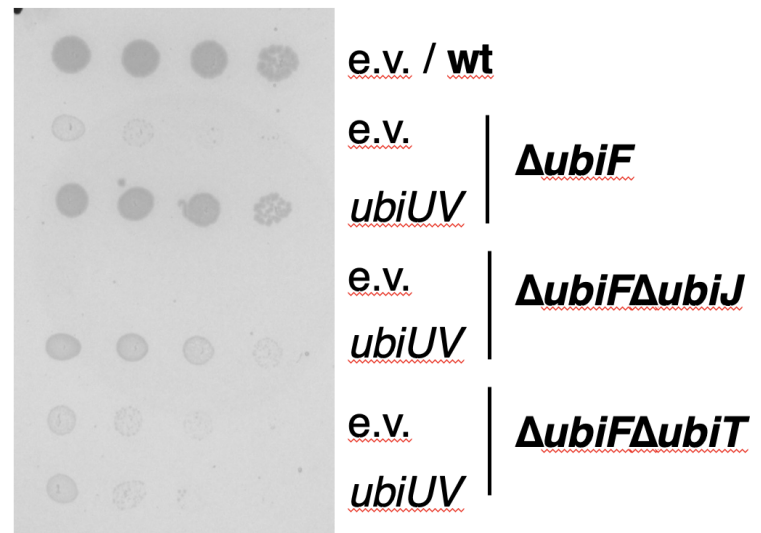
A

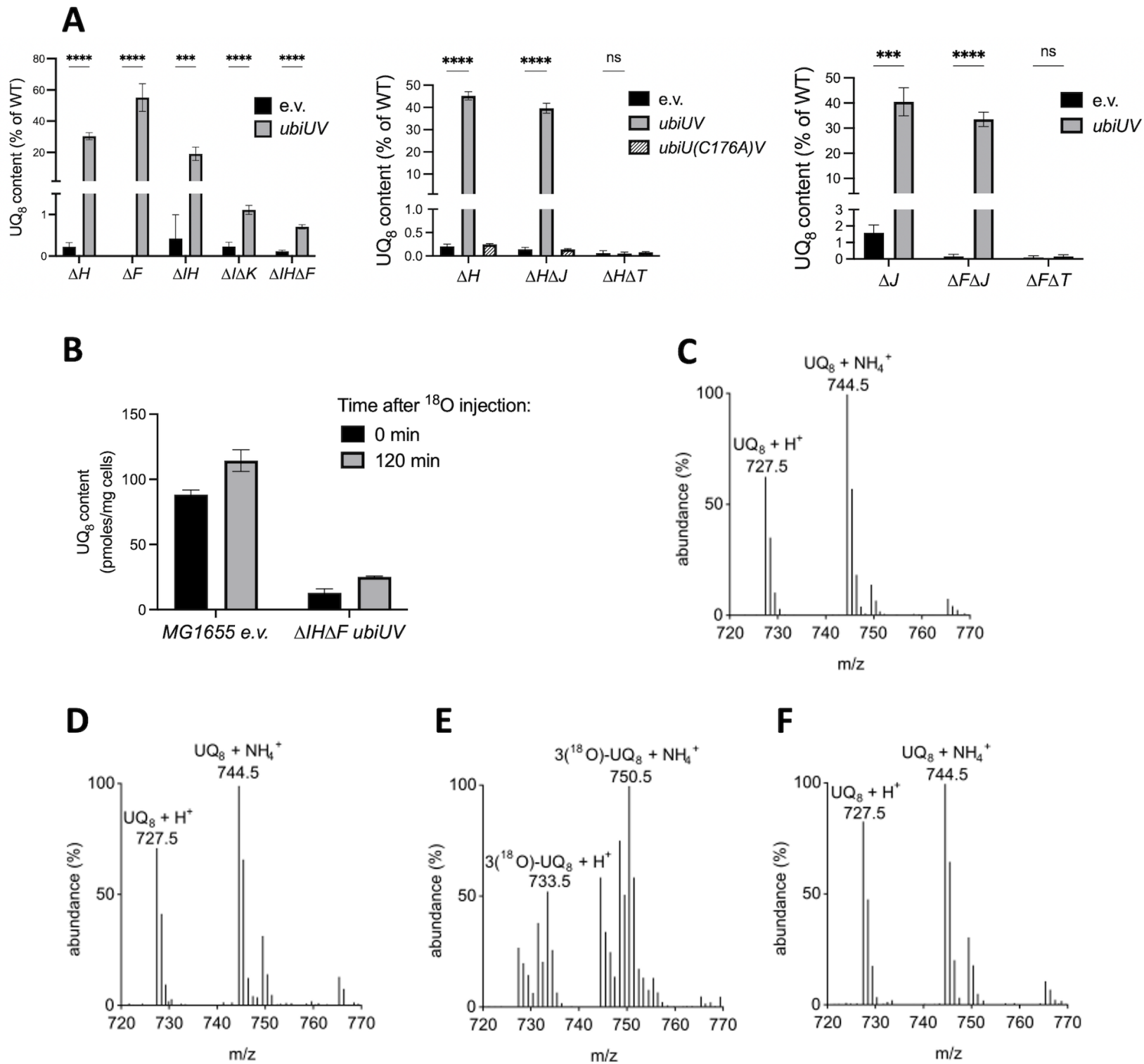


B

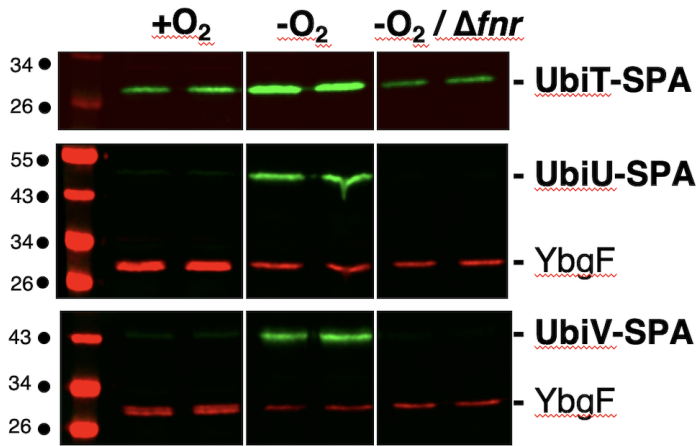


C

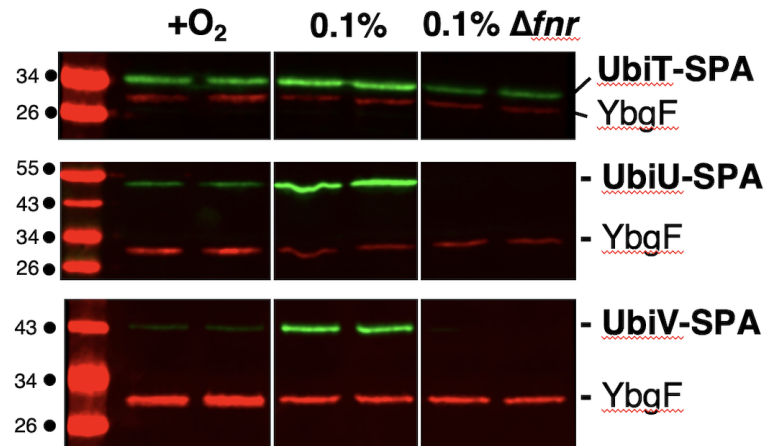




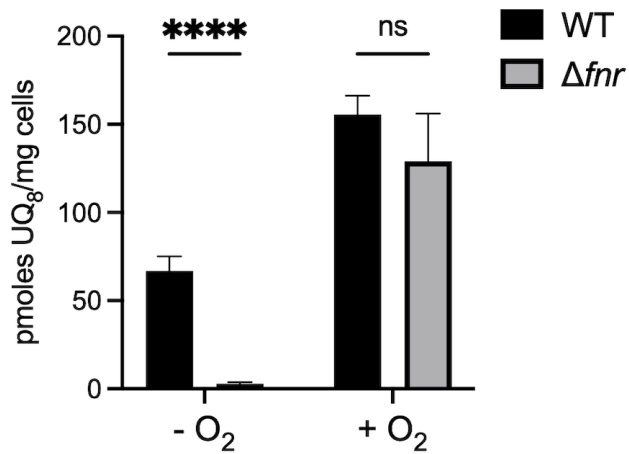
A



B



C



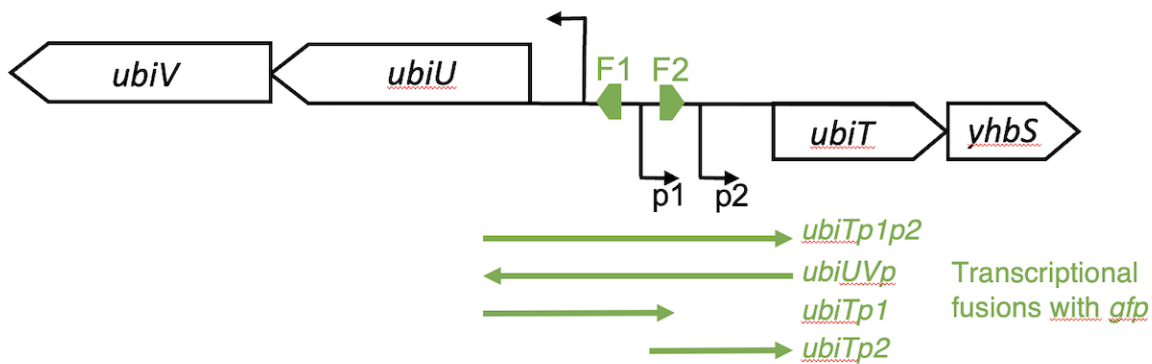
A

1 **cat**AATTTTCTCTGAAGGTTGCGCTATCAAAACGCAAAAATGTTAA**C**GAACTGGGATTTTAGTTA
 66 ACCTTGCTGCGACAATTT**TTGATTTAAGGCAG**TTAAAGTTGTATTGGTGGTAGC**A**GCAATTT**CAT**
 131 ATGGAATTG**TTGATTTATACCGC**TATGTTATTTTTCTGATATGGCAAAAATAGGATG**A**TTGTTGAA
 196 ACAGGGAGTAAAACTC**gta**

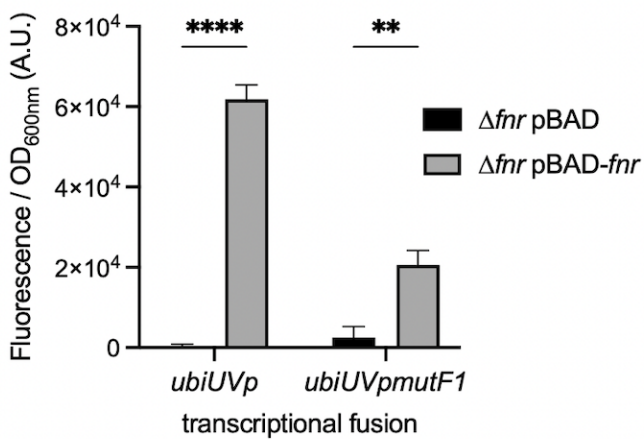
ubiUVp ←
ubiTp1 →
ubiTp2 →

F1 site
 mutF1: GATGA
 F2 site
 mutF2: CATGA
 mutΔF2

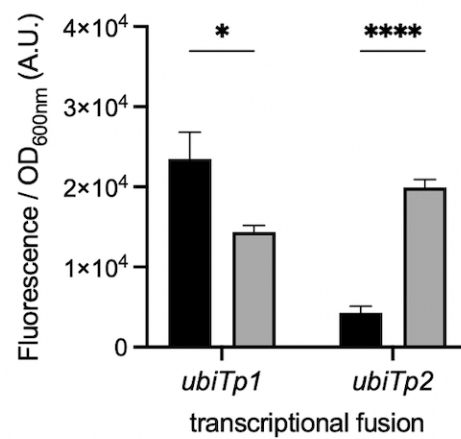
B



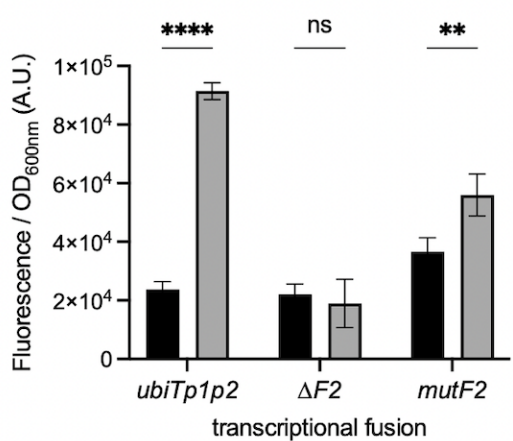
C



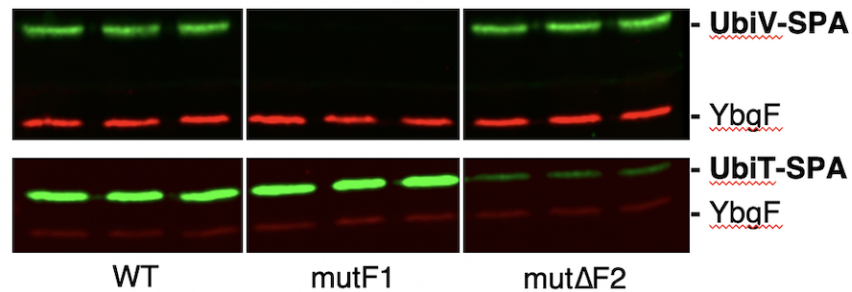
D

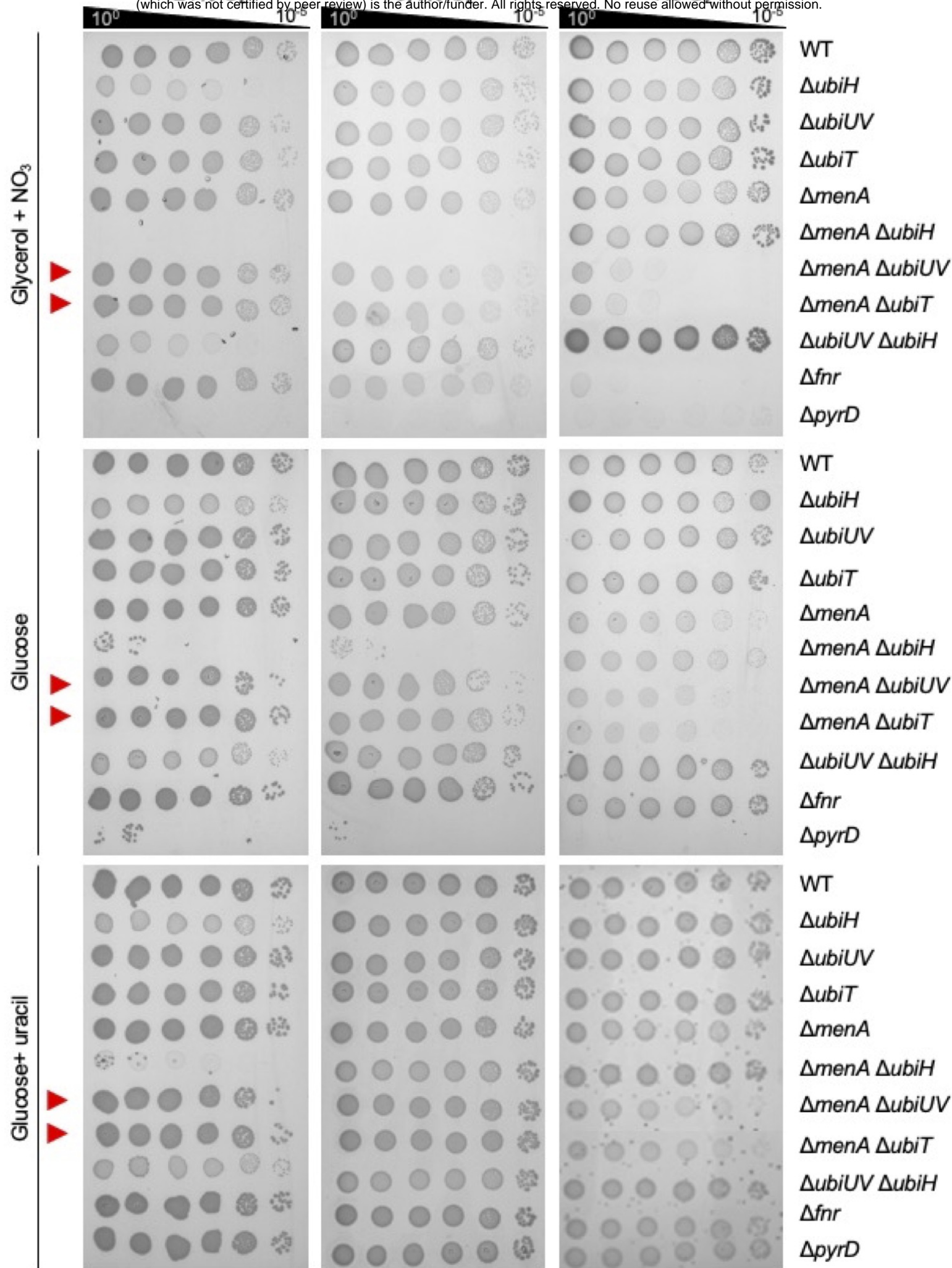


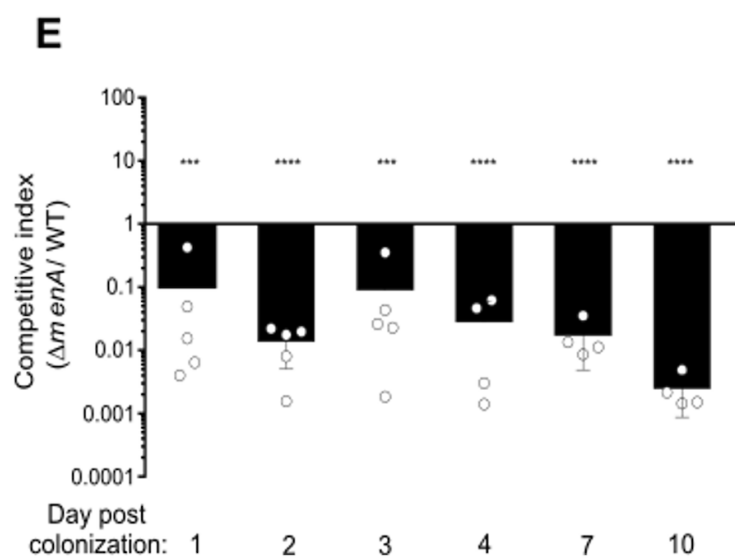
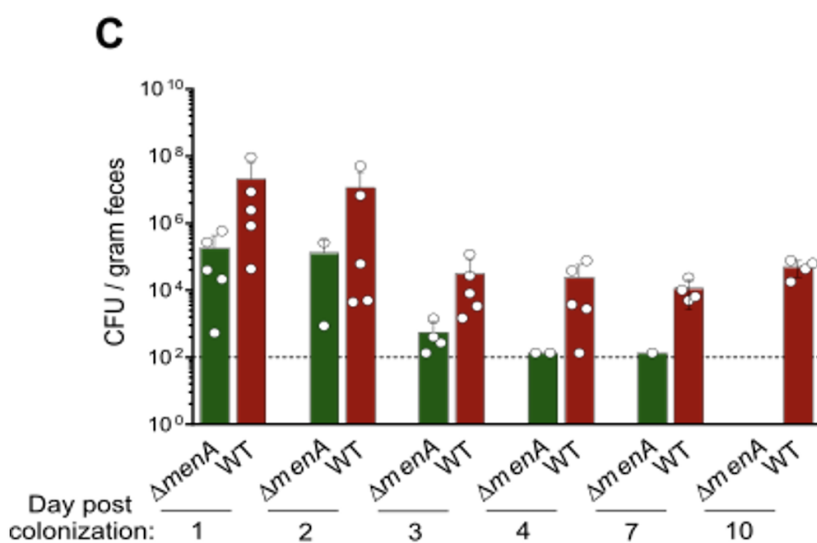
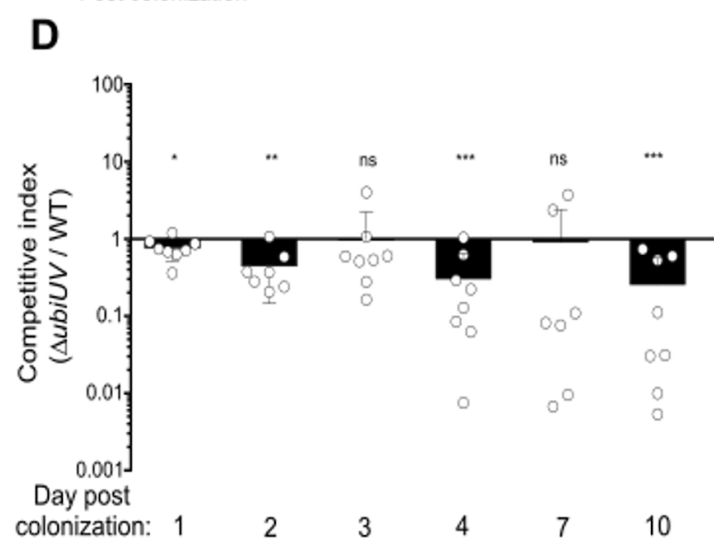
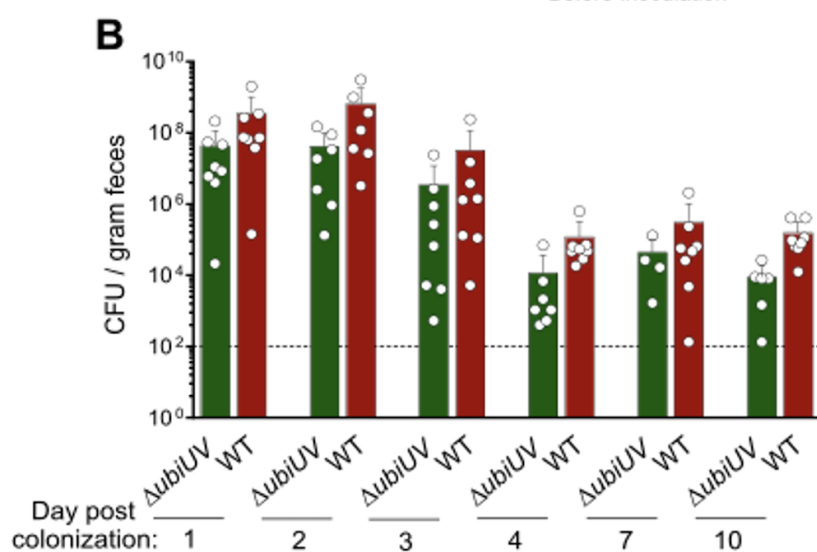
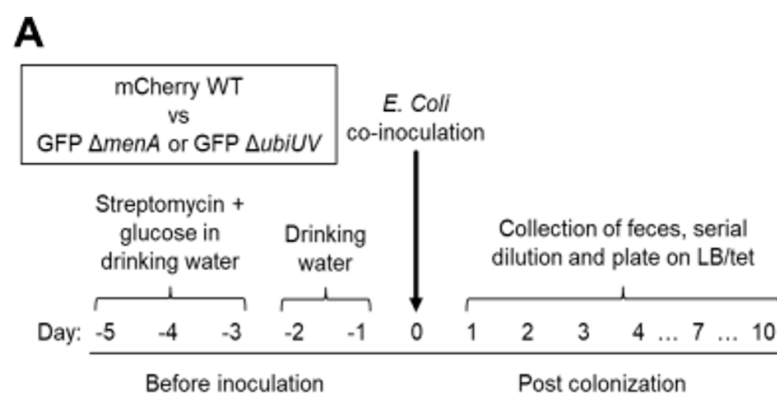
E



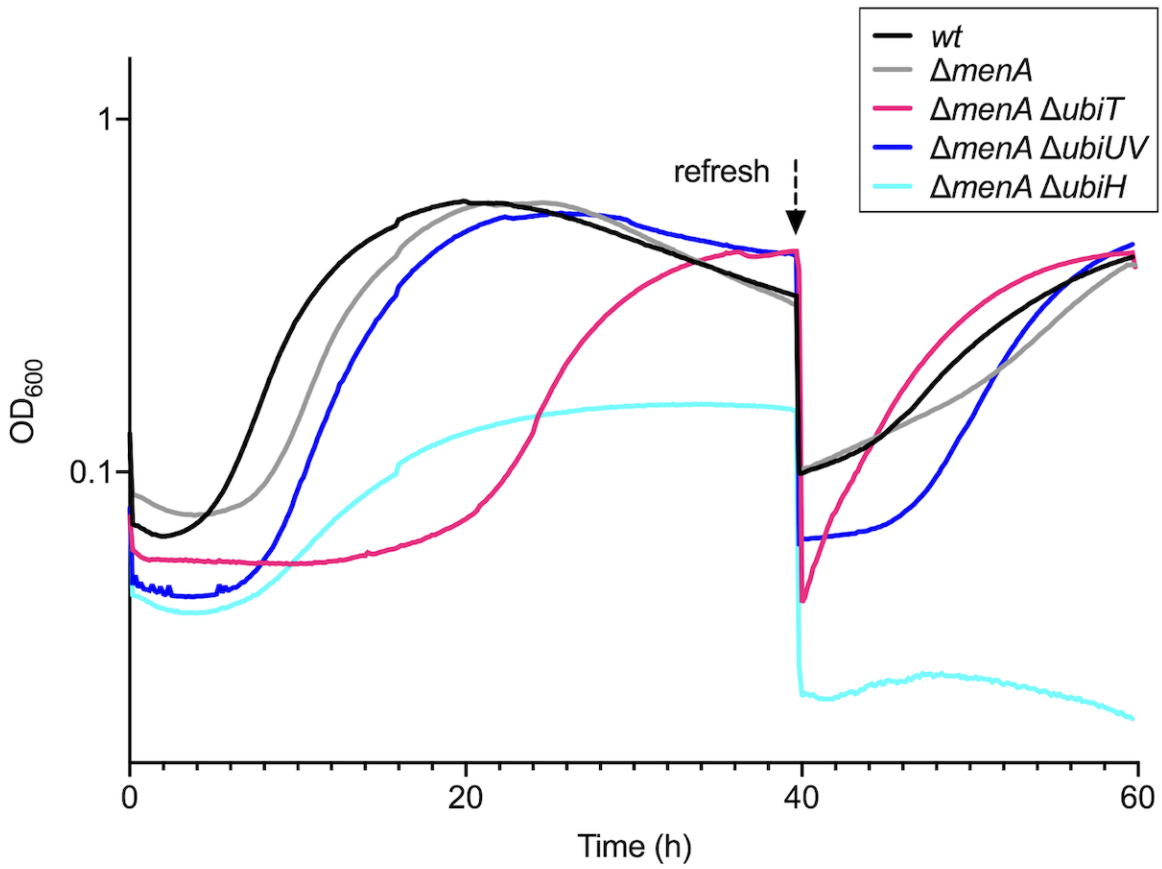
F







A



B

